

สมบัติแม่เหล็กของ  $\text{Sm}_2\text{Co}_{17}$  และ  $\text{Sm}_2\text{Co}_{17}\text{N}_x$  ในเฟสรวมโบฮีตรัล



น.ส.นฤมล สุวรรณจันทร์ดี

วิทยานิพนธ์นี้เป็นส่วนหนึ่งของการศึกษาดำเนินการตามหลักสูตรปริญญาวิทยาศาสตรมหาบัณฑิต

สถาบันวิทยบริการ

บัณฑิตวิทยาลัย จุฬาลงกรณ์มหาวิทยาลัย


จุฬาลงกรณ์มหาวิทยาลัย

พ.ศ. 2538

ISBN 974-631-691-5

ลิขสิทธิ์ของบัณฑิตวิทยาลัย จุฬาลงกรณ์มหาวิทยาลัย

MAGNETIC PROPERTIES OF  $\text{Sm}_2\text{Co}_{17}$  AND  $\text{Sm}_2\text{Co}_{17}\text{N}_x$   
IN THE RHOMBOHEDRAL PHASE



Miss Narumon Suwonjandee

A Thesis Submitted in Partial Fulfillment of the Requirements  
for the Degree of Master of Science

Department of Physics  
Graduate School

Chulalongkorn University

1995

ISBN 974-631-691-5

Thesis Title            Magnetic properties of  $\text{Sm}_2\text{Co}_{17}$  and  $\text{Sm}_2\text{Co}_{17}\text{N}_x$  in  
                                 the rhombohedral phase  
By                            Miss Narumon Suwonjandee  
Department            Physics  
Thesis Advisor        Professor Thamrong Methasiri, F.D.  
Thesis Co-advisor    Professor I-Ming Tang, Ph.D.



---

Accepted by the Graduate School, Chulalongkorn University in  
Partial Fulfillment of the Requirements for the Degree of Master of Science.

*Santi Thoongsuwan*

..... Dean of Graduate School  
(Associate Professor Santi Thoongsuwan, Ph.D.)

Thesis Committee

*Somphong Chatraphorn* Chairman

.....  
(Assistant Professor Somphong Chatraphorn, M.Sc.)

*T. Methasiri*

..... Thesis Advisor  
(Professor Thamrong Methasiri, F.D.)

*I-Ming Tang*

..... Thesis Co-advisor  
(Professor I-Ming Tang, Ph.D.)

*Phavanantha*

..... Member  
(Associate Professor Phathana Phavanantha, Ph.D.)

*Mayuree Natenapit*

..... Member  
(Assistant Professor Mayuree Natenapit, Ph.D.)

## C625364 : MAJOR PHYSICS

KEY WORD: RHOMBICEDRAL PHASE / COERCIVE FORCE / REMANENT MAGNETIZATION

$\text{Sm}_2\text{Co}_{17}$  /  $\text{Sm}_2\text{Co}_{17}\text{N}_x$

NARUMGN SUWONJANDEE : MAGNETIC PROPERTIES OF  $\text{Sm}_2\text{Co}_{17}$  AND  $\text{Sm}_2\text{Co}_{17}\text{N}_x$

IN THE RHOMBICEDRAL PHASE. THESIS ADVISOR : PROF. THAMRONG  
METHASIRI, F.D. THESIS CO-ADVISOR : PROF. I-MING TANG, Ph.D.  
69 pp. ISBN 974-631-691-5

The nitrogenation of  $\text{Sm}_2\text{Fe}_{17}$  is required to raise the Curie temperature above the temperature range in which the magnets will be used. The raising of the Curie temperature is accompanied by beneficial increases in the other magnetic properties. In this study, we investigate whether the same beneficial increases occurs when  $\text{Sm}_2\text{Co}_{17}$  undergoes nitrogenation. We find that the coercivity is 1.4 kOe, the remanent magnetization is 1.1 KG, and the energy product is 0.24 MGOe after nitrogenation. These magnetic properties of  $\text{Sm}_2\text{Co}_{17}\text{N}_x$  are very low comparing with the other groups and are not as great as  $\text{Sm}_2\text{Fe}_{17}$ . The reason may be that  $\text{Sm}_2\text{Co}_{17}$  has some impurities due to the preparation, and the  $\text{Sm}_2\text{Co}_{17}\text{N}_x$  is inhomogeneous, due to the nitrogen coming through the powder does not reach equilibrium.

สถาบันวิทยบริการ  
จุฬาลงกรณ์มหาวิทยาลัย

ภาควิชา..... วัสดุศาสตร์  
สาขาวิชา..... วัสดุศาสตร์  
ปีการศึกษา..... ๒๕๒๕

ลายมือชื่อนิสิต..... วิมล สุวรรณ  
ลายมือชื่ออาจารย์ที่ปรึกษา..... อ.ค. เมธาสิริ  
ลายมือชื่ออาจารย์ที่ปรึกษาร่วม..... I-Ming Tang

พิมพ์ต้นฉบับบทคัดย่อวิทยานิพนธ์ภายในกรอบสี่เหลี่ยมนี้เพียงแผ่นเดียว

นฤมล สุวรรณจันทร์ดี : สมบัติแม่เหล็กของ  $\text{Sm}_2\text{Co}_{17}$  และ  $\text{Sm}_2\text{Co}_{17}\text{N}_x$   
ในเฟสรูทไมอิตริล (MAGNETIC PROPERTIES OF  $\text{Sm}_2\text{Co}_{17}$  AND  $\text{Sm}_2\text{Co}_{17}\text{N}_x$   
IN THE RHCMECHEDRAL PHASE) อ.ที่ปรึกษา : ศ.ดร.ธำรง เมธาศิริ,  
อ.ที่ปรึกษาร่วม : ศ.ดร.อิ-มิ่ง ถัง, 69 หน้า. ISBN 974-631-691-5

การเติมไนโตรเจนแก่สาร  $\text{Sm}_2\text{Fe}_{17}$  จะทำให้อุณหภูมิคูรีเพิ่มสูงขึ้นกว่าอุณหภูมิ  
ที่ใช้แม่เหล็กนั้นอยู่ การเพิ่มของอุณหภูมิคูรีนี้เนื่องมาจากการเปลี่ยนสมบัติแม่เหล็กอื่น ๆ  
ในการศึกษานี้ เราจะพิจารณาว่าเมื่อเราเติมไนโตรเจนแก่สาร  $\text{Sm}_2\text{Co}_{17}$  สมบัติ  
แม่เหล็กจะเปลี่ยนในลักษณะเดียวกันหรือไม่ พบว่าหลังจากที่เติมไนโตรเจนแก่สารแล้ว  
แรงผลักแม่เหล็กมีค่า 1.4 กิโลเออร์สเตด สนามแม่เหล็กค้างมีค่า 1.1 กิโลเกาส์  
และพลังงานสูงสุดมีค่า 0.24 เมกกะเกาส์เออร์สเตด สมบัติแม่เหล็กของสาร  
 $\text{Sm}_2\text{Co}_{17}\text{N}_x$  นี้เมื่อเปรียบเทียบกับผู้วิจัยกลุ่มอื่น จะมีค่าต่ำกว่าและไม่สูงเท่ากับที่มีใน  
สาร  $\text{Sm}_2\text{Fe}_{17}$  สาเหตุอาจเนื่องมาจากสาร  $\text{Sm}_2\text{Co}_{17}$  มีสารเจือปนอยู่มาก ซึ่ง  
อาจเกิดจากขั้นตอนในการเตรียมสาร และอีกสาเหตุหนึ่งคือ สาร  $\text{Sm}_2\text{Co}_{17}\text{N}_x$   
มีความไม่สม่ำเสมอซึ่งอาจเกิดจากไนโตรเจนที่เข้าไปในสารยังไม่ถึงจุดสมดุล



สถาบันวิทยบริการ  
จุฬาลงกรณ์มหาวิทยาลัย

ภาควิชา ฟิสิกส์  
สาขาวิชา ฟิสิกส์  
ปีการศึกษา ๒๕๓๕

ลายมือชื่อนิติ Ann Sittay  
ลายมือชื่ออาจารย์ที่ปรึกษา ดร. ธำรง  
ลายมือชื่ออาจารย์ที่ปรึกษาร่วม Dr. Ming Tang

## ACKNOWLEDGMENTS



The author would like to express her deep appreciation to Prof. Thamrong Methasiri, and Prof. I-Ming Tang for their continuous encouragement, guidance and help during the course of the work as thesis advisor and co-advisor, respectively. She also wishes to express her thanks to Assistant Prof. Somphong Chatraphorn and Dr. Pongthip Vinothai for their help in various ways.

She would like to thank Mr. Prasert Kaewpimpa, and other authorities at the Scientific and Technological Research Equipment Center, and also at the Metallurgy and Materials Science Research Institute. Finally, she would like to express her sincere thank to the Metallurgy and Materials Science Research Institute for financial support.

สถาบันวิทยบริการ  
จุฬาลงกรณ์มหาวิทยาลัย

## TABLE OF CONTENTS



	Page
ABSTRACT IN ENGLISH.....	iv
ABSTRACT IN THAI.....	v
ACKNOWLEDGMENTS .....	vi
TABLE OF CONTENTS .....	vii
LIST OF FIGURES.....	ix
LIST OF TABLES.....	xi
<b>CHAPTER I INTRODUCTION (GENERAL PROPERTIES)</b>	
Magnetic properties .....	1
Types of magnetism .....	6
Hysteresis curve .....	10
Energy product .....	10
Outline of thesis .....	13
<b>CHAPTER II RARE-EARTH MAGNETS</b>	
The development of rare-earth permanent magnets.....	14
Application of Sm-Co magnets.....	16
The interaction between rare-earth-transition metal (RE-TM) compounds.....	18
Exchange interactions in RE-TM compounds.....	19
<b>CHAPTER III MAGNETIC PROPERTIES OF RARE-EARTH MAGNETS</b>	
Introduction.....	22
Magnetic structure.....	22
Magnetic properties.....	24
Insertion of H,C or N in the RE-TM compounds.....	28
Magnetic property of inserted RE-TM (H,C,N) compounds.....	32

CHAPTER IV	EXPERIMENT DETAILS	
	A. Nitrogenation .....	33
	B. Characterization .....	35
	C. Magnetic property measurements .....	35
CHAPTER V	RESULT AND DISCUSSION	
	A. Nitrogenation .....	37
	B. Simple Characterization .....	42
	C. Magnetic properties .....	48
CHAPTER VI	CONCLUSION .....	58
REFERENCES	.....	61
APPENDIX A	.....	63
APPENDIX B	.....	64
CURRICULUM VITAE	.....	69



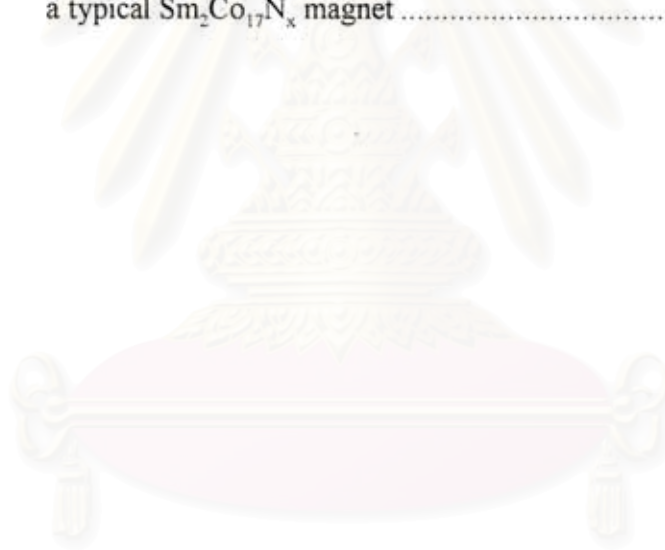
สถาบันวิทยบริการ  
จุฬาลงกรณ์มหาวิทยาลัย



## LIST OF FIGURES

		Page
Fig. 1.1	The torque on a current loop in an external magnetic field.....	3
Fig. 1.2	The torque on a bar magnet in an external magnetic field .....	4
Fig. 1.3	Different forms of magnetic behavior .....	7
Fig. 1.4	Magnetic induction <b>B</b> vs. applied field <b>H</b> hysteresis loop for a ferromagnetic material .....	11
Fig. 1.5	The energy product (BH) curve of a permanent magnet .....	12
Fig. 2.1	The Sm-Co magnets have been used in medical aid .....	17
Fig. 3.1	Crystal structure of RE <sub>2</sub> TM <sub>17</sub> compounds .....	23
Fig. 3.2	Saturation magnetization of the binary intermetallic RE-TM magnets .....	26
Fig. 3.3	Curie temperatures of the binary intermetallic RE-TM magnets .....	27
Fig. 3.4	Curie temperature ternary compounds formed by the absorption of H,C,N by the binary RE-TM compounds .....	29
Fig. 3.5	Th <sub>2</sub> Zn <sub>17</sub> crystal structure showing the tetragonal sites into which H ions can enter .....	30
Fig. 3.6	Schematic structure representation of Nd <sub>2</sub> Fe <sub>17</sub> N <sub>3</sub> .....	31
Fig. 4.1	LINBERG/BLUEM 1700°C crucible furnace .....	34
Fig. 4.2	WALKER SCIENTIFIC MAGNETIC HYSTERESISGRAPH.....	36
Fig. 5.1	Percentage weight of nitrogen absorbed as a function of nitrogenating time.....	40
Fig. 5.2	Mole fraction of nitrogen absorbed as a function of nitrogenating time.....	41
Fig. 5.3	A typical XRD pattern for Sm <sub>2</sub> Co <sub>17</sub> N <sub>x</sub> .....	43

Fig. 5.4	Changes in the Lattice Parameters as a function of nitrogenation time.....	45
Fig. 5.5	Photographs of the grains used to determine grain sizes .....	47
Fig. 5.6	Hysteresis Loop of a typical $\text{Sm}_2\text{Co}_{17}\text{N}_x$ specimen .....	49
Fig. 5.7	Saturation magnetization of $\text{Sm}_2\text{Co}_{17}\text{N}_x$ specimens as a function of nitrogenation time .....	51
Fig. 5.8	Remanent magnetization of $\text{Sm}_2\text{Co}_{17}\text{N}_x$ specimens as a function of nitrogenation time for various processing temperatures.....	53
Fig. 5.9	Coercive Force of $\text{Sm}_2\text{Co}_{17}\text{N}_x$ specimens as a function of nitrogenation time for various processing temperatures .....	54
Fig. 5.10	A plot of the energy product BH for different values of B of a typical $\text{Sm}_2\text{Co}_{17}\text{N}_x$ magnet .....	56



สถาบันวิทยบริการ  
จุฬาลงกรณ์มหาวิทยาลัย

## LIST OF TABLE

	Page
Table 1.1 Susceptibilities and permeabilities of various elements .....	8
Table 3.1 Intrinsic properties of $\text{Sm}_2\text{Fe}_{17}$ .....	25
Table 5.1 Mass of samples before and after nitrogenation .....	39
Table 5.2 Lattice parameters ( a,c ) changes as a function of nitrogenating time .....	44
Table 5.3 Particle ( grain ) sizes for specimens nitrogenated for different time durations and temperatures .....	46
Table 5.4 Magnetic Properties of $\text{Sm}_2\text{Co}_{17}\text{N}_x$ .....	50
Table 5.5 The relationship between the coercive force ( $H_c$ ) and particle sizes .....	55
Table 5.6 $(BH)_{\text{max}}$ of the nitrided $\text{Sm}_2\text{Co}_{17}$ .....	57
Table 6.1 Comparison of the magnetic properties .....	60

สถาบันวิทยบริการ  
จุฬาลงกรณ์มหาวิทยาลัย

## CHAPTER I

### INTRODUCTION



#### Magnetic properties

When considering magnetic materials, the necessary quantities that represent the response of these materials to the field are the magnetic field, the magnetic induction, the magnetic moment, and the magnetization. These should first be defined.

##### A. Magnetic field, $\mathbf{H}$

A magnetic field is produced whenever there is electrical charge in motion. This can be due to an electrical current flowing in a conductor. A magnetic field is also produced by a permanent magnet. In this case there is no conventional electric current, but there are the orbital motions and spins of electrons within the permanent magnet material. The magnetic field exerts a force on both current-carrying conductors and permanent magnets. The unit of magnetic field strength is defined in terms of the generation current, amp/metre (Jiles, 1991).

##### B. Magnetic induction, $\mathbf{B}$

When a magnetic field  $\mathbf{H}$  has been generated in a medium by a current, the response of the medium is its magnetic induction  $\mathbf{B}$ , (Jiles, 1991) sometimes called the flux density. The flux density in webers/metre<sup>2</sup> or testla is also known as the magnetic induction  $\mathbf{B}$ . All media will respond with some induction and the relation between magnetic induction and magnetic field is a property called the **permeability**,  $\mu$  of the medium. In many media  $\mathbf{B}$  is a linear function of  $\mathbf{H}$ . In particular in free space we can write

$$\mathbf{B} = \mu_0 \mathbf{H} \quad (1.1)$$

where  $\mu_0$  is the permeability of free space and has the value of  $4\pi \times 10^{-7}$  tesla-metres/ampere and is independent of  $\mathbf{H}$ . However in other media, particularly ferromagnets and ferrimagnets,  $\mathbf{B}$  is no longer a linear function of  $\mathbf{H}$ . They can still be related by the permeability of the medium  $\mu$  through the equation,

$$\mathbf{B} = \mu \mathbf{H} \quad (1.2)$$

but where  $\mu$  is not necessarily independent of  $\mathbf{H}$ .

### C. Magnetic moment, $\mathbf{m}$

The magnetic moment  $\mathbf{m}$  of a current loop dipole is  $i$  time  $A$ ,  $\mathbf{m} = iA$ . ( where  $A$  is the area enclosed by the loop ( see Figure 1.1. )). In the case of a bar magnet, as in Figure 1.2.,  $\mathbf{m} = \mathbf{pl}$ , where  $\mathbf{p}$  is the pole strength in amp metres and  $l$  is the dipole length in metres (Jiles, 1991). The torque acting on the dipole in the presence of a magnetic field in free space is given by  $\boldsymbol{\tau} = \mathbf{m} \times \mathbf{B}$ . Therefore the magnetic moment can be expressed as the maximum torque on a magnetic dipole  $\tau_{\max}$  divided by  $\mathbf{B}$

$$\mathbf{m} = \tau_{\max} / \mathbf{B} \quad (1.3)$$

where the magnetic momentum is measured in amp-meter<sup>2</sup>, which is equal to a current loop or to a bar magnet.

สถาบันวิทยบริการ  
จุฬาลงกรณ์มหาวิทยาลัย

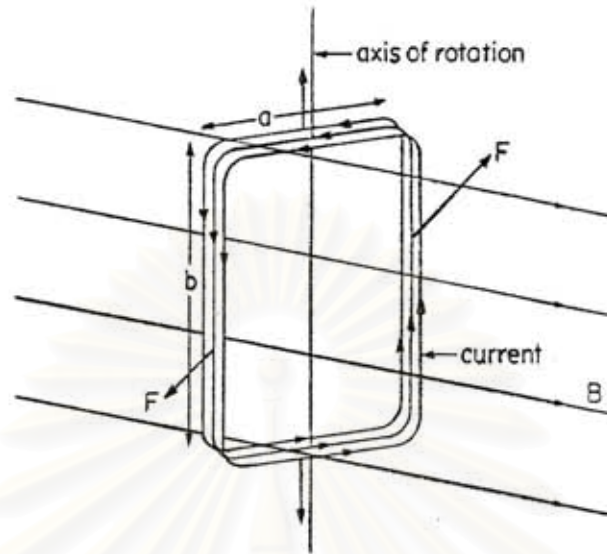


Figure 1.1a.

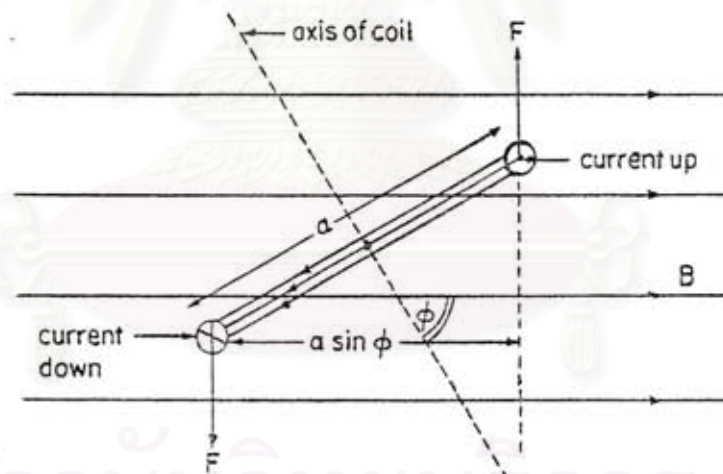


Figure 1.1b.

FIGURE 1.1 The torque on a current loop in an external magnetic field:

(a) side view, and (b) top view.

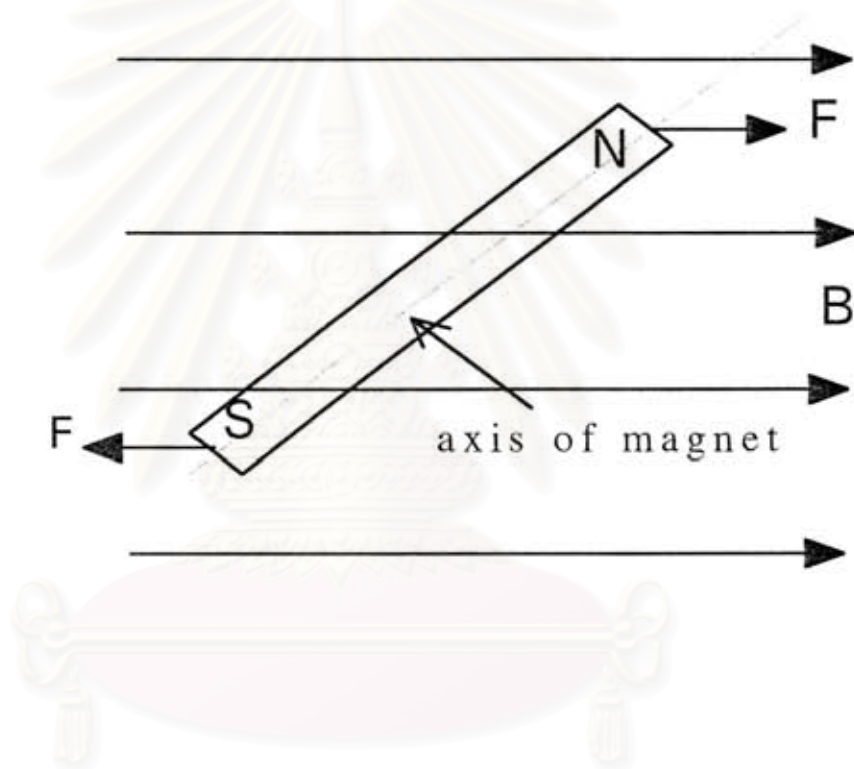


FIGURE 1.2 The torque on a bar magnet in an external magnetic field.

สถาบันวิทยบริการ  
จุฬาลงกรณ์มหาวิทยาลัย

#### D. Magnetization, $\mathbf{M}$

The magnetization can be defined as the magnetic moment per unit volume of a solid,

$$\mathbf{M} = \mathbf{m}/V \quad (1.4)$$

For a bar magnet with flux density  $\phi$  at the centre, dipole length  $l$  and with cross-sectional area  $A$ , where the magnetic moment  $\mathbf{m}$  is given by  $\mathbf{m} = \phi l/\mu_0$ , the magnetization  $\mathbf{M}$  is given by  $\mathbf{M} = \mathbf{m}/Al$ . Hence,

$$\mathbf{M} = \phi/\mu_0 A = \mathbf{B}/\mu_0 \quad (1.5)$$

We can see that the magnetization  $\mathbf{M}$  and magnetic field  $\mathbf{H}$  contribute to the magnetic induction in a similar way. If both magnetization and magnetic field are present then the magnetic induction is simply the vector sum of these two, i.e.,

$$\mathbf{B} = \mu_0(\mathbf{H} + \mathbf{M}) \quad (1.6)$$

#### E. Permeability and susceptibility, $\mu$ , $\kappa$

The permeability  $\mu$  and susceptibility  $\kappa$  are defined as

$$\mu = \mathbf{B}/\mathbf{H} \quad (1.7)$$

and 
$$\kappa = \mathbf{M}/\mathbf{H} \quad (1.8)$$

Since  $\mathbf{B}$  and  $\mathbf{M}$  may or may not be linear functions of  $\mathbf{H}$ , depending on the type of material or medium, the permeability and susceptibility may be functions of  $\mathbf{H}$ .

Sometimes it is convenient to use the relative permeability of a medium, denoted  $\mu_r$ , given by

$$\mu_r = \mu/\mu_0 \quad (1.9)$$



The relative permeability is a measure of the intensity of the induced magnetic field which is dimensionless. The relative permeability is closely related to the susceptibility given by

$$\mu_r = \kappa + 1 \quad (1.10)$$

### Types of magnetism

Magnetic materials can be classified into 5 major groups ( as shown in Figure 1.3 ) according to their susceptibility.

#### A. Diamagnetism

Diamagnetism is produced when an external magnetic field acting on the atoms of a material slightly unbalances their orbiting electrons and creates small magnetic dipoles within the atoms which oppose the applied field. This makes the net magnetic moment of each atom in a material zero because of mutually cancelling electronic movements within the atom. The diamagnetic materials have a very small negative magnetic susceptibility of the order of  $\kappa = -10^{-5}$  and their relative permeability are slightly less than one. Examples are copper (Cu), bismuth (Bi), lead (Pb) and galium (Ga) (Parker, 1990 ; Smith, 1993).

#### B. Paramagnetism

Paramagnetism is produced by the parallel alignment of individual magnetic dipole moments of atoms or molecules in an applied magnetic field. The paramagnetic effect in materials disappears when the applied magnetic field is removed. Since thermal agitation randomizes the directions of the magnetic dipoles, an increase in temperature decreases the paramagnetic effect. Paramagnetism produces magnetic susceptibilities in material ranging from about  $10^{-6}$  to  $10^{-2}$  while relative permeability is slightly greater than one. Many salt and metals exhibit paramagnetism. The values of susceptibility and relative permeability of both diamagnetic and paramagnetic materials are shown in Table 1.1 (Jiles, 1991 ; Smith, 1993).

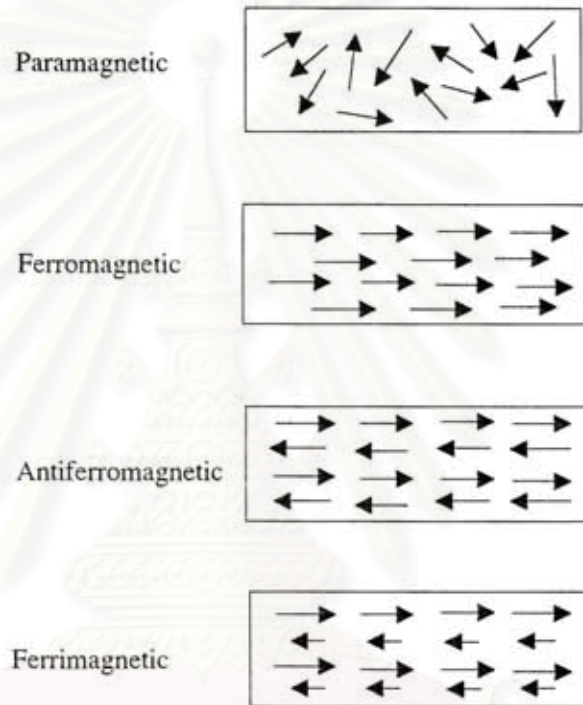


FIGURE 1.3 Different forms of magnetic behavior.

สถาบันวิทยบริการ  
จุฬาลงกรณ์มหาวิทยาลัย

TABLE 1.1

Susceptibilities and permeabilities of various elements

		$\kappa$	$\mu_r$
Diamagnets	Bi	$-1.31 \times 10^{-6}$	0.99983
	Be	$-1.85 \times 10^{-6}$	0.99998
	Ag	$-2.02 \times 10^{-6}$	0.99997
	Au	$-2.74 \times 10^{-6}$	0.99996
	Ge	$-0.56 \times 10^{-6}$	8 0.99999
	Cu	$-0.77 \times 10^{-6}$	0.99999
Paramagnets	$\beta$ -Sn	$0.19 \times 10^{-6}$	1.00000
	W	$6.18 \times 10^{-6}$	1.00008
	Al	$1.65 \times 10^{-6}$	1.00002
	Pt	$21.04 \times 10^{-6}$	1.00026
	Mn	$66.10 \times 10^{-6}$	1.00083

สถาบันวิทยบริการ  
จุฬาลงกรณ์มหาวิทยาลัย

### C. Ferromagnetism

Materials that have large magnetization even in the absence of magnetic field are called ferromagnetic. In these materials, individual atoms have a net magnetic moment due to unbalanced electron spins, as for paramagnetism, but in addition the interatomic spacing lies within a critical range, which gives rise to exchange forces causing parallel alignment between neighboring atoms. As temperature is increased a point is reached where thermal agitation overcomes the exchange forces. This critical temperature is called the Curie point, above which the material becomes paramagnetic. The most important ferromagnetic elements are iron (Fe), cobalt (Co), and nickel (Ni) (Parker, 1990).

The ferromagnetic properties of the transition elements Fe, Co, and Ni are due to the way the spins of the inner unpaired electrons are aligned in their crystal lattices. In Fe, Co, and Ni the unpaired inner 3d electrons are responsible for the ferromagnetism which these elements exhibit. The iron atom has four unpaired 3d electrons, the cobalt atom three, and the nickel atom two.

### D. Antiferromagnetism

In the presence of a magnetic field, magnetic dipole moments of atoms of antiferromagnetic materials align themselves in opposite directions to each other, so no spin moment is observed. Such a substance shows a slight positive susceptibility. This susceptibility increases with temperature up to a critical temperature, the Neel point, at which the ordering breaks down, and normal paramagnetic response is observed. Examples are chromium (Cr) and manganese (Mn) (Parker, 1990 ; Smith, 1993).

### E. Ferrimagnetism

This is a special case of antiferromagnetism. Ferrimagnetism may be considered to result when two sublattice atomic moments, though being antiparallel have magnetization of different magnitudes. A net magnetization occurs in one direction. As a group ferrimagnetic materials are called ferrites (Parker, 1990).

### Hysteresis curve

The most common way to represent the magnetic properties of a ferromagnetic material is by a plot of magnetic induction  $\mathbf{B}$  for various field strengths  $\mathbf{H}$ . Alternatively plots of magnetization  $\mathbf{M}$  against  $\mathbf{H}$  are used. They contain the same information since  $\mathbf{B} = \mu_0(\mathbf{H}+\mathbf{M})$ . From the hysteresis curve in Figure 1.4, as the applied field increases from zero,  $\mathbf{B}$  increases from zero along curve OA until **saturation induction**  $\mathbf{B}_s$  is reached at point A. Upon decreasing the applied field to zero, the original magnetization curve is not retraced. There remains a magnetic flux density called the **remanent induction**  $\mathbf{B}_r$  (point C). To decrease the magnetic induction to zero, a reverse (negative) applied field of the amount  $\mathbf{H}_c$ , called the **coercive force**, must be applied (point D). If the negative applied field is increased still more, the materials will reach saturation induction in the reverse field at point E. Upon removing the reverse field, the magnetic induction will return to the remanent induction at point F. Upon application of a positive applied field, The  $\mathbf{B}$ - $\mathbf{H}$  curve will follow FGA to complete a loop. This magnetization loop is referred to as a **hysteresis loop**, and its internal area is a measure of energy lost or the work done by the magnetizing and demagnetizing cycle.

### Energy product

The hard magnetic materials should be magnetized in a magnetic field strong enough to orient their magnetic domains in the direction of the applied field. Some of the applied energy of the field is converted into potential energy which is stored in the permanent magnet produced. Hard magnetic materials are difficult to demagnetize once magnetized. The demagnetizing curve for a hard magnetic material is chosen as the second quadrant of its hysteresis loop, and can be used for comparing the strengths of permanent magnets.

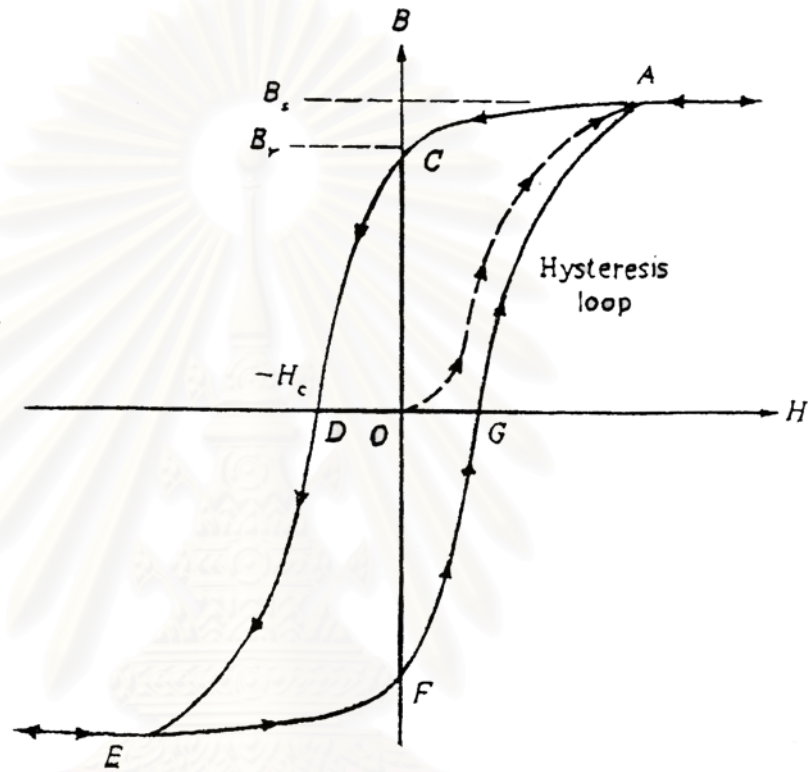


FIGURE 1.4 Magnetic induction  $\mathbf{B}$  vs. applied field  $\mathbf{H}$  hysteresis loop for a ferromagnetic material.

จุฬาลงกรณ์มหาวิทยาลัย

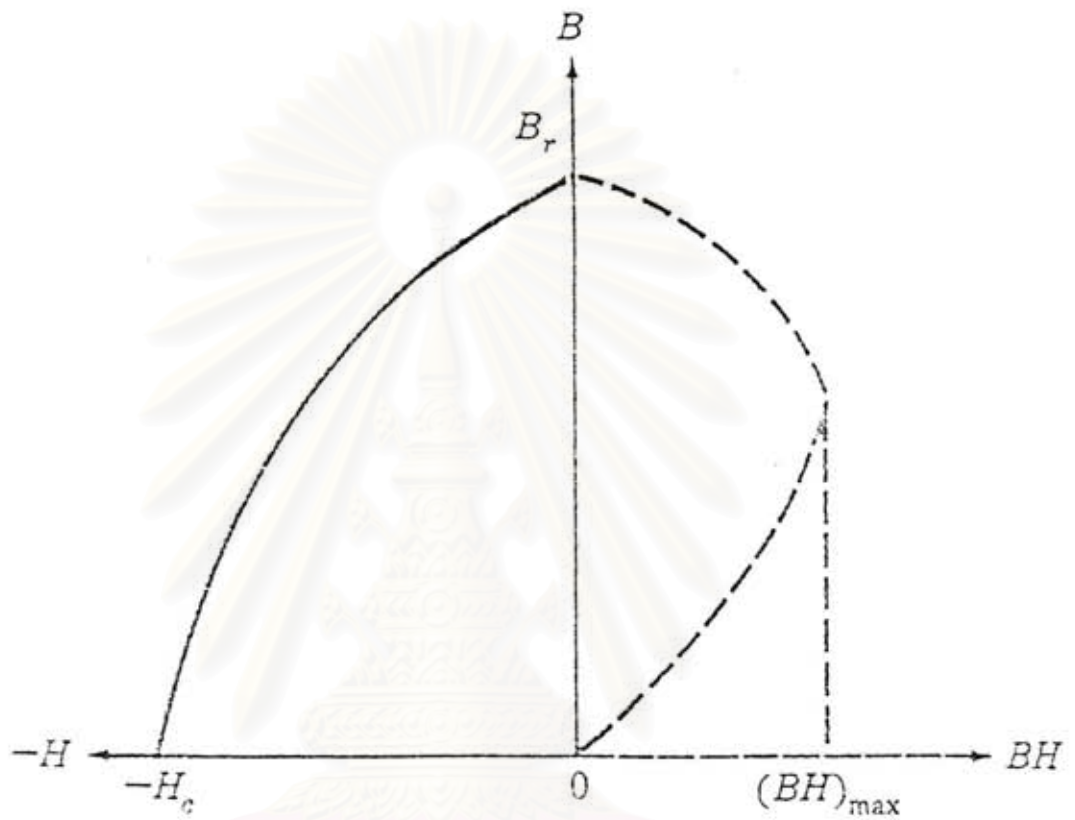


FIGURE 1.5 The energy product (BH) curve of a permanent magnetic material.

สถาบันวิทยบริการ  
จุฬาลงกรณ์มหาวิทยาลัย

The magnetic potential energy of a permanent magnetic material is measured by its maximum energy product, which is the maximum value of the product of **B** and **H** determined from the demagnetizing curve of the material. Figure 1.5 shows the external energy (BH) curve for a permanent magnetic material and its maximum energy product,  $(BH)_{\max}$ . Basically, the maximum energy product of the material is the area occupied by the largest rectangle that can be inscribed in the second quadrant of the hysteresis loop of the material.

### Outline of thesis

The purpose of this thesis is to study the magnetic properties of the samarium-cobalt ( Sm-Co ) compounds especially of  $\text{Sm}_2\text{Co}_{17}$ . We started by diffusing the nitrogen atoms into the  $\text{Sm}_2\text{Co}_{17}$  compounds and see how the interstitial nitrogen affects the lattice parameters ( a,c ). We determine the amount of nitrogen atoms going into the compounds. After pressing the compounds into pellets, the magnetic properties are measured. This is done by looking at the hysteresis curve for each specimen.

In Chapter I, we have reviewed some basic properties of magnetic materials, and some characteristic which can be obtained from hysteresis curve. The magnetic properties and interactions of the RE-TM compounds are discussed in Chapter II and III. In Chapter IV, we present the experimental details. The result and discussion are given in chapter V. The direction of future work is given in Chapter VI.

จุฬาลงกรณ์มหาวิทยาลัย



## CHAPTER II



### RARE-EARTH MAGNETS

#### The development of rare-earth permanent magnets

The development of high energy magnets has gathered steam during this century. The first magnets, the spinel ferrite,  $\text{Fe}_3\text{O}_4$  (magnetite or lodestone) have a very low energy product  $(\text{BH})_{\text{max}}$  (the product of the field intensity  $\mathbf{H}$  and the magnetic induction field  $\mathbf{B}$ ). The first significant increase in the energy product was seen in the creation of the hexaferrites,  $\text{SrFe}_{12}\text{O}_{20}$  (with a  $(\text{BH})_{\text{max}}$  of  $28 \text{ kJ/m}^3$ ). The next increase was seen in the fabrication of the Alnico alloys with energy product of  $83 \text{ kJ/m}^3$ . A doubling of the energy product to between  $130\text{-}180 \text{ kJ/m}^3$  was achieved with the development of the  $\text{SmCo}_5$  magnets. A further increase to  $200\text{-}240 \text{ kJ/m}^3$  is obtained in the  $\text{Sm}(\text{Co,Fe,Cu,Zr})_2$  magnets. Even higher energy products are obtained in the Nd-Fe-B magnets. Present research is now looking at the development of  $\text{RE-TM}_2\text{N}_4$  magnets with high energy products.

The development of the families of "rare-earth permanent magnets" (RE-PM) has been going on for past 30 years. As pointed out above, the RE-PM surpassed all earlier magnets, with the best values of energy product and coercivity (or coercive force  $H_c$ , the field needed to bring the induction field back to zero). The RE-PM are metal (alloys) magnets in which the magnetic components are 3d-transition metals (TM) and elements of the rare-earth group (RE), i.e., the 4f-elements. These magnets can be divided into two major subgroups: RE-Co-based magnets (especially Sm-Co) and RE-Fe-based magnets. The RE-Co of the 1:5 and 2:17 families are outstanding new permanent magnets. The  $\text{RECo}_5$  and also  $\text{RE}_2\text{Co}_{17}$  in which RE is a light-RE, e.g. Ce, Pr, Nd, Sm or Y have attracted much interests. Studies on the anisotropy using single crystal or oriented powders showed that  $\text{YCo}_5$  and

$\text{RECo}_5$  compounds have extremely large crystal anisotropies with a single easy axis of magnetization. The  $\text{RE}_2\text{Co}_{17}$  with Sm, Er and Tm were shown to have an easy axis except for  $\text{Y}_2\text{Co}_{17}$  which shows to be an easy-basal-plane anisotropy. Fine particle theory suggested that micron size powders of these  $\text{RECo}_5$  and  $\text{RE}_2\text{Co}_{17}$  compounds should have very high coercivity. In powders produced by mechanical grinding,  $H_{ci}$  ( the intrinsic coercive force ) reaches only 5-10% of their anisotropy fields ( Strnat and Strnat , 1991 ).

The development of sintering techniques has lead to fully dense and stable  $\text{SmCo}_5$  magnets. Similar types of magnets have the Sm replaced by blends (mischmetal ) of Ce, Pr, Nd and La. To obtain high coercive fields  $H_c$  , it is necessary that some Sm is included in the mixture. The partial substitution of Cu for Co in  $\text{SmCo}_5$  and in  $\text{CeCo}_5$  led to high coercive force without having to work with finely powder materials. Fabrication methods that work well for  $\text{SmCo}_5$  , when applied to  $\text{Sm}_2\text{Co}_{17}$  , yields only coercivities in the 1-3 kOe range. High coercivity was obtained in sintered  $\text{Sm}(\text{Co,Tm})_8$  magnets by adding some Fe and Cu. Further improvement was seen in the discovery that by adding a little Zr, in  $\text{Sm}(\text{Co,Fe,Cu,Zr})_7$  and then heat-treating the alloy, coercivities of about 6.5 kOe (520 kA/m) could be achieved.

In the quasi-binary intermetallics  $\text{RE}_2(\text{Co}_{1-x}\text{Fe}_x)_{17}$  , modest ion additions stabilize the easy-c-axis anisotropy in all light-RE system ( except Nd ), increase the saturation magnetization  $M_s$  and depress  $T_c$  ( the temperature at which spontaneous magnetization begins ) only slightly. In 1976, the energy product for  $\text{SmCo}_5$  magnets, sintered  $\text{Sm}(\text{Co,Fe,Mn,Cr})_{8.5}$  , was up to  $240 \text{ kJ/m}^3$  with a  $H_c$  of 12 kOe. The best energy product, greater than  $240 \text{ kJ/m}^3$  , was achieved with 1.5 wt% Zr and  $z=7.4$ . Adding titanium and hafnium to similar alloys with  $\text{RE} = \text{Ce}$  or  $\text{Sm}$  lead to comparable beneficial effects on the microstructure and coercivity. Using more zirconium ( up to 3 wt% ) and longer heat-treatments give much higher coercivity, 10 to 25 kOe. The best energy product was  $265 \text{ kJ/m}^3$  with  $z=7.67$  (Strnat and Strnat, 1991).

All RE-PM containing more than two elements are multiphase, nonequilibrium metallurgical systems with complex microstructures. The binary RE-PM intermetallics or alloys rich in Co or Fe compounds having the low-moment (light-RE) Ce, Pr, Nd or Sm or having nonmagnetic La and Y, have high spontaneous magnetization. The light-RE are coupled ferromagnetically to the Co or Fe, thus the high saturation magnetization  $M_s$ . The heavy-RE are coupled antiferromagnetically to the Co and Fe. This leads to the lower  $M_s$ . Among the families of RE-PM compounds, the  $T_c$  for  $RE_2Co_{17}$  is 800 to 950 °C, for  $RECo_5$  the  $T_c$  is high, while for  $RE_2Fe_{17}$ , the  $T_c$ 's are low. However, by introducing some boron to form ternary compounds  $RE_2Fe_{14}B$ , the  $T_c$  are raised by 200-300 °C over the corresponding  $RE_2Fe_{17}$  values. By introducing interstitial nitrogen, hydrogen and carbon, the lattice parameters of  $RE_2Fe_{17}$  are increased as are their  $T_c$  and  $M_s$ .

The second group, i.e., RE-Fe based, uses cheaper and more plentiful raw materials than Sm-Co. They, e.g., Nd-Fe-B, have higher energy density at room temperature. However, they have greater stability problems at room and elevated temperatures than the Sm-Co magnets.

#### Application of Sm-Co magnets

The magnetic properties such as high coercivity, high temperature stability and high energy product can be translated into substantial size, weight and performance advantage in a number of devices. D.C. motors have been developed which use the inside-out type of construction in which the windings are in the stationary outer member and the inner structure consists of a rotating magnet. Electric wrist watches have been made using these magnets. The more powerful Sm-Co magnets allow a reduction in current consumption. These magnets are being used in microwave components such as the travelling wave tubes. It has been possible to bring down the overall size and the weight of these devices without affecting their performance.



Figure 2.1a.

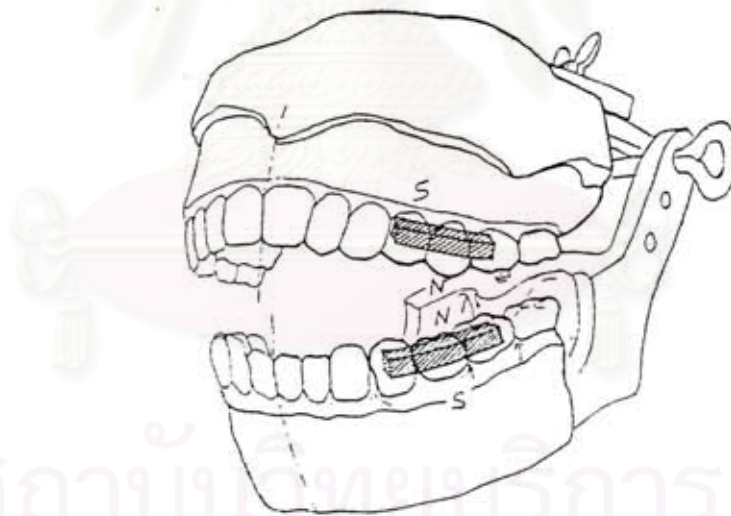


Figure 2.1b.

Figure 2.1 The Sm-Co magnets have been used in medical aid.

(2.1a) Light plastic shoulder harness with embedded Sm-Co magnets.

(2.1b) Sm-Co wafers embedded in dentures.

Furthermore, these Sm-Co magnets have been used for medical aid. In Figure ( 2.1 a ) , two powerful Sm-Co magnets are placed inside a plastic shoulder harness. Two similar magnets arranged in a repelling configuration are kept in a collar. This arrangement gives a gentle lift to the head. This new aid permits the user to move his head in a limited way, provides a steady and gentle stretching action and is much more comfortable to wear than a stiff collar. These magnets have been used in dentures also. Small Sm-Co wafers are placed under teeth 4 to 7 on both the dentures and on both the sides. The magnets are kept in repelling configuration. Figure ( 2.1 b ) shows the positioning of the two Sm-Co magnets. These magnets cause the dentures to press gently against the gums.

#### The interaction between rare-earth-transition metal (RE-TM) compounds

The binary RE-TM compounds, where TM is a 3d-metal, are very interesting now. One reason is that their magnetic behaviors arise from interactions involving unpaired electrons of very different characteristics. On the one hand there are f-electrons with a small spatial extent which lead to a magnetism that is well described in terms of many-body ionic states. On the other hand there are d-electrons which participate in metallic bonding. In these RE-TM compounds, there are three types of interactions, namely, TM-TM interactions which are direct exchange interactions between the 3d spins, RE-RE interactions which are indirect interactions proceeding by the 4f-5d-5d-4f mechanism, and RE-TM interactions which are also indirect, being a combination of the interatomic 4f-5d and interatomic 5d-3d exchange interaction (Duc et al., 1993). With the RE-TM intermetallics, we have a magnetic system which combines the large magnetic interaction and high Curie temperature associated with the 3d-electrons of the TM and the large magnetocrystalline anisotropy and magnetostriction associated with the 4f-electrons of the RE elements, to produce outstanding permanent magnet properties (Ballou, 1994).

According to the Hund's rule, the coupling between the RE and TM moments will be ferromagnetic for the light-RE elements and antiferromagnetic for the heavy-RE elements. In the TM rich RE-TM compounds with a magnetic RE element and with TM being either Fe or Co, a collinear ferrimagnetism is usually obtained with a Curie temperature given by

$$T_c = (1/2) \{ T_M + T_R + [(T_M - T_R)^2 + 4 T_{RM}^2]^{1/2} \} \quad (2.1)$$

where  $T_M$ ,  $T_R$  and  $T_{RM}$  represent the contributions to  $T_c$  due to TM-TM, RE-RE and RE-TM exchange interactions. For the RE-TM<sub>5</sub> compound, GdNi<sub>5</sub>, the Curie temperature is 29 K. This should be compared with the  $T_c$  ( 987 K ) of YCo<sub>5</sub>. Assuming that the RE- RE interactions are not strongly dependent on the nature of the alloyed TM element, these values of  $T_c$  would indicate that in RECo<sub>5</sub> compounds the Co-Co interactions are larger than the RE-RE interactions. Comparing the Curie temperatures of YCo<sub>5</sub> ( 987 K ) and GdCo<sub>5</sub> ( 1293 K ), one finds that  $T_{RM} = T_{MM}/3$ , showing that the RE-TM interactions are also dominant over the RE-RE interactions (Ballou, 1994). Thus, Isnard et al., ( Isnard, Miraglia, Fruchart, Soubeyroux et al., 1994 ) use the following expression for  $T_c$  containing only a term which varies linearly with the Fe-Fe distance

$$T_c = a + b \langle d_{Fe-Fe} \rangle \quad (2.2)$$

to fit the observed  $T_c$ 's of RE<sub>2</sub>Fe<sub>17</sub>N<sub>x</sub> magnets. This is consistent with the idea that only the interaction between the Fe and Fe ions are important.

#### Exchange interactions in RE-TM compounds

As was just pointed, there are three types of exchange interactions in RE-TM intermetallics, i.e., RE-RE interactions between the magnetic moments within the RE sublattice, TM-TM interactions between the magnetic moments of the TM

sublattice, and RE-TM intersublattice interactions, as we discussed above. The effect of these RE-TM interactions is to maintain the RE magnetism at room temperatures and above. It is standard to express these different types of interactions as effective exchanges of the Heisenberg type (Jiles, 1991 ; Duc et al, 1993) :

$$H_{ex} = -2 \sum_{\text{nearest-neighbour}} A_{ij} S_i S_j \quad (2.3)$$

where  $A_{ij}$  is the exchange coupling between neighboring spin  $S_i$  and  $S_j$ . There are three different kinds of spin pairs in RE-TM compounds, so the exchange interactions are described by three parameters  $A_{TT}$ ,  $A_{RT}$ , and  $A_{RR}$ .

Within a mean-field approach, the exchange interactions are related to the molecular field action on the spin moments. The molecular fields of the RE and TM sublattices can be written as (Duc et al, 1993) :

$$B_R = B_o + \eta_{RR} M_R + \eta_{RT} M_T \quad , \quad (2.4)$$

$$B_T = B_o + \eta_{TT} M_T + \eta_{TR} M_R \quad (2.5)$$

where  $B_o$  is the external magnetic field,  $M_R$  is the magnetic moment of the RE sublattice per unit mass,  $M_T$  is that of the TM sublattice,  $\eta_{ij}$  are the macroscopic molecular field coefficients.

The Brillouin function is used to describes the temperature dependence of each sublattice moment:

$$M_R(T) = M_R(0) B_J \left( \frac{M_R(0) H_R(T)}{k_B T} \right) \quad (2.6)$$

$$M_T(T) = M_T(0) B_J \left( \frac{M_T(0) H_T(T)}{k_B T} \right) \quad (2.7)$$

where  $M_R(0)$  and  $M_T(0)$  are the magnetic moments of RE and TM at zero temperature, respectively.  $H_R(T)$  and  $H_T(T)$  are the molecular fields of rare-earth and

iron sublattices at temperature  $T$ .  $J_R$  and  $J_T$  are the individual RE and TM total angular momenta, and  $B_J(x)$  is defined as (Jiles, 1991) :

$$B_J(x) = \frac{2J+1}{2J} \coth \left[ \frac{(2J+1)}{2J} x \right] - \frac{1}{2J} \coth \left( \frac{x}{2J} \right) \quad (2.8)$$

For most RE-TM intermetallic compounds the exchange interactions favor ferromagnetic RE and TM moment arrangement for the light-RE and antiferromagnetic alignment for the heavy-RE. The molecular field coefficient  $\eta_{ij}$  are related to  $A_{ij}$  through (Duc et al, 1993):

$$\eta_{RR} = 2 Z_{RR} A_{RR} (g-1)^2 / g^2 \mu_B^2 N_R \quad (2.9)$$

$$\eta_{RT} = Z_{RT} A_{RT} (g-1) / g \mu_B^2 N_T \quad (2.10)$$

$$\eta_{TR} = Z_{TR} A_{RT} (g-1) / g \mu_B^2 N_R \quad (2.11)$$

$$\eta_{TT} = Z_{TT} A_{TT} (g-1) / 2 g \mu_B^2 N_T \quad (2.12)$$

where  $Z_{RR}$  and  $Z_{RT}$  are the numbers of RE and TM nearest neighbors of an RE ion, respectively, and  $Z_{TR}$  and  $Z_{TT}$  are the numbers of RE and TM neighbors of a TM ion.  $N_R$  and  $N_T$  are the numbers of RE and TM atoms per formula unit,  $g$  is the Lande' factor of the RE ion. The terms  $\eta_{RR}M_R$  in equation (2.4) and  $\eta_{TT}M_T$  in equation (2.5) are largely dominated by  $\eta_{RT}M_T$  and  $\eta_{TR}M_R$ , respectively.

จุฬาลงกรณ์มหาวิทยาลัย



## CHAPTER III



### MAGNETIC PROPERTIES OF RARE-EARTH MAGNETS

#### Introduction

In this chapter we will consider the magnetic properties of rare-earth iron (RE-Fe) compounds, especially the samarium-iron compound  $\text{Sm}_2\text{Fe}_{17}$ . We will see how the interaction mechanisms are affected by the insertion of hydrogen (H), carbon (C), and nitrogen (N) into the interstitial sites within the crystal structure of these compounds and how the magnetic properties are changed.

#### Magnetic structure

The discovery of  $\text{Nd}_2\text{Fe}_{14}\text{B}$  in 1983 had led to an extensive search for new high performance magnetic materials. The important intrinsic magnetic properties for such a material are the Curie temperature  $T_c$ , the spontaneous magnetization  $M_s$ , and the coercive force  $H_c$ . In recent years, many studies have been conducted on the rare-earth transition (RE-TM) intermetallic compounds RE-Fe. The  $\text{RE}_2\text{Fe}_{17}$  compounds have the highest  $M_s$  among all RE-Fe compounds. In general, they exist across the RE series in two related crystallographic modifications. The light-RE ( Ce, Pr, Nd, Sm and Tb ) form the rhombohedral  $\text{Th}_2\text{Zn}_{17}$  structure and the heavy-RE ( Dy, Ho, Er, Tm and Lu ) and Y form the hexagonal  $\text{Th}_2\text{Ni}_{17}$  structure, with different stacking of the layers along  $c$  axis. Both the crystal structures are shown in Figure 3.1. Figure (3.1a) shows the  $\text{Th}_2\text{Zn}_{17}$  structure in which the Sm atoms occupy the single RE site (6c), while the Fe atoms occupy four inequivalent sites 6c, 9d, 18f and 18h. Figure (3.1b) shows the hexagonal  $\text{Th}_2\text{Ni}_{17}$  structure.

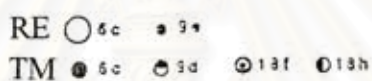
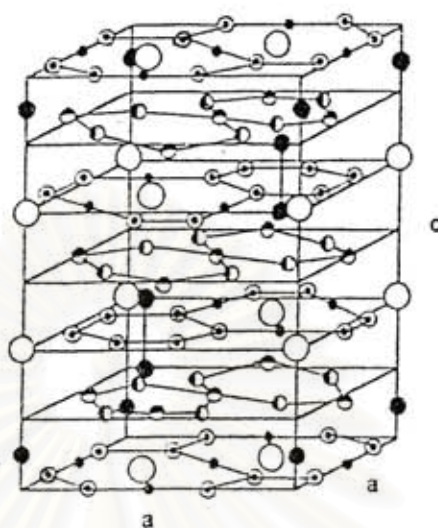


Figure 3.1a.

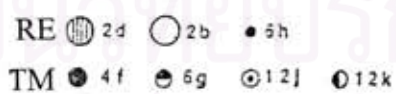
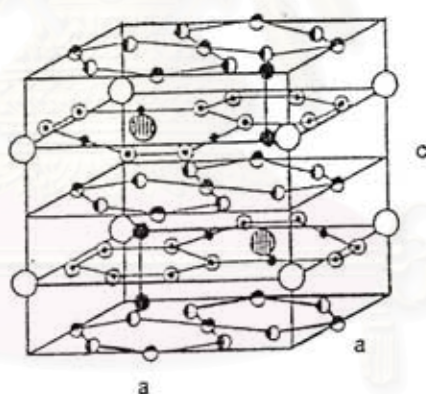


Figure 3.1b.

FIGURE 3.1 Crystal structure of  $\text{RE}_2\text{TM}_{17}$  compounds.

- (3.1a) The rhombohedral  $\text{Th}_2\text{Zn}_{17}$  structure formed when the RE is a light member of the lanthanide rare earth series.
- (3.1b) The hexagonal  $\text{Th}_2\text{Ni}_{17}$  structure formed when the RE is a heavy member of the lanthanide series.

### Magnetic properties

The intrinsic properties of  $\text{Sm}_2\text{Fe}_{17}$  are summarized in Table 3.1. We shall now discuss each property:

#### A. Spontaneous magnetization $M_s$

Of the binary RE-TM intermetallic compounds, only those rich in Fe or Co and particularly the ferromagnetic compounds of the low-moment light-RE and of some nonmagnetic have a sufficiently high spontaneous magnetization. The room temperature saturation values are summarized in Figure 3.2 (Strnat and Strnat, 1991). The peculiarities of the 4f-3d exchange interaction are evident: the light-RE couples ferromagnetically to Fe (Co) leading high saturation magnetization  $M_s$  which declines as the temperature increases, while the heavy-RE couples antiferromagnetically to the Fe (Co) resulting in low  $M_s$  which rises with increasing temperature.

#### B. Curie temperature $T_c$

$\text{RE}_2\text{Fe}_{17}$  Curie temperatures are too low for practical magnets. The  $\text{RE}_2\text{Co}_{17}$  are the best, while the  $\text{RE}_2\text{Fe}_{17}$  Curie temperatures are too low for practical magnets. However, introducing some boron to form the ternary compounds  $\text{RE}_2\text{Fe}_{14}\text{B}$  will raise  $T_c$  over the corresponding  $\text{RE}_2\text{Fe}_{17}$  values. Figure 3.3 summarized the Curie temperatures of the same families of RE-TM compounds (Strnat and Strnat, 1991).

สถาบันวิทยบริการ  
จุฬาลงกรณ์มหาวิทยาลัย

TABLE 3.1  
Intrinsic properties of  $\text{Sm}_2\text{Fe}_{17}$

Samples	Structure	a [°A]	c [°A]	T <sub>c</sub> [K]
<sup>a</sup> $\text{Sm}_2\text{Fe}_{17}$	rhombohedral	8.55	12.44	423
<sup>a</sup> $\text{Sm}_2\text{Fe}_{17}\text{N}_x$	rhombohedral	8.74	12.65	753
<sup>a</sup> $\text{Sm}_2\text{Fe}_{17}\text{C}_{0.4}$	rhombohedral	8.61	12.46	490
<sup>a</sup> $\text{Sm}_2\text{Fe}_{17}\text{C}_{0.7}$	rhombohedral	8.62	12.46	503
<sup>a</sup> $\text{Sm}_2\text{Fe}_{17}\text{C}_{0.9}$	rhombohedral	8.63	12.47	524
<sup>b</sup> $\text{Sm}_2\text{Fe}_{17}$	rhombohedral	8.54	12.43	389
<sup>b</sup> $\text{Sm}_2\text{Fe}_{17}\text{H}_{2.2}$	rhombohedral	8.65	12.51	527
<sup>b</sup> $\text{Sm}_2\text{Fe}_{17}\text{C}_{1.1}$	rhombohedral	8.63	12.46	495
<sup>b</sup> $\text{Sm}_2\text{Fe}_{17}\text{N}_{2.3}$	rhombohedral	8.73	12.64	749
<sup>c</sup> $\text{Sm}_2\text{Fe}_{17}$	rhombohedral	8.54	12.43	390
<sup>c</sup> $\text{Sm}_2\text{Fe}_{17}\text{C}_2$	rhombohedral	8.73	12.65	680
<sup>c</sup> $\text{Sm}_2\text{Fe}_{17}\text{N}_{2.3}$	rhombohedral	8.73	12.64	749
<sup>d</sup> $\text{Sm}_2\text{Fe}_{17}$	rhombohedral	8.55	12.44	385
<sup>d</sup> $\text{Sm}_2\text{Fe}_{17}\text{H}_x$	rhombohedral	8.68	12.55	565
<sup>e</sup> $\text{Sm}_2\text{Fe}_{17}\text{N}_{2.5}$	rhombohedral	8.74	12.67	750

a : Data from Kou, et al. 1991.

b : Data from Otani, et al. 1990.

c : Data from Altounian, et al. 1993.

d : Data from Isnard, Miraglia, Soubeyroux, et al. 1994.

e : Data from Buschow, et al. 1990.

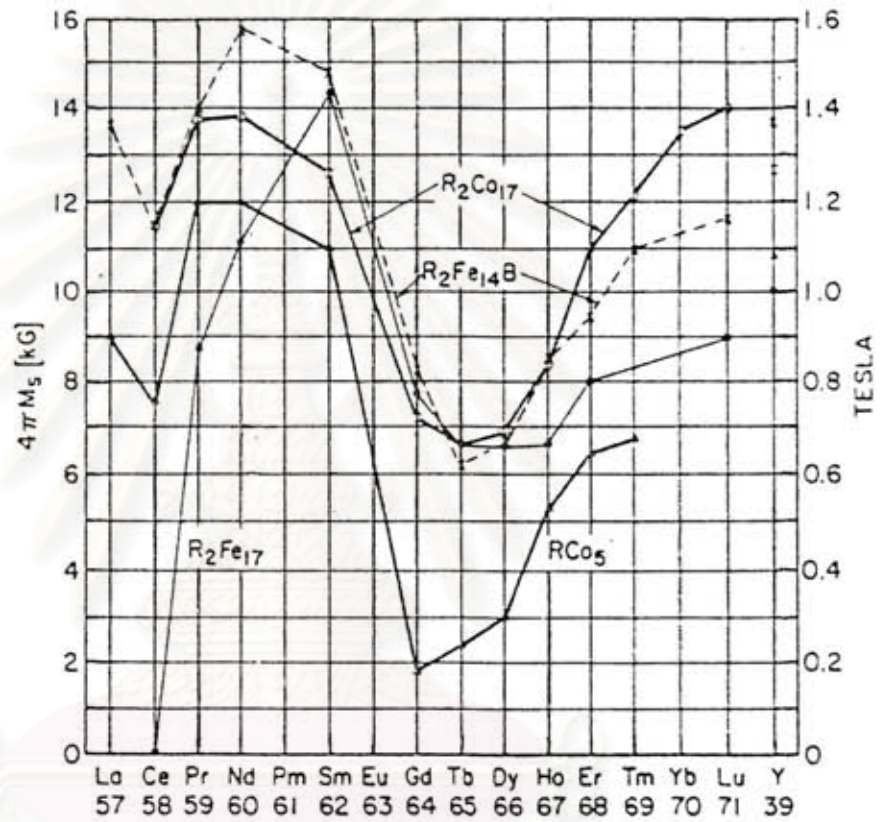


FIGURE 3.2 Saturation magnetization of the binary intermetallic RE-TM magnets. ( Data from Strnat, et al. 1991.)

สถาบันวิจัยปรอท  
จุฬาลงกรณ์มหาวิทยาลัย

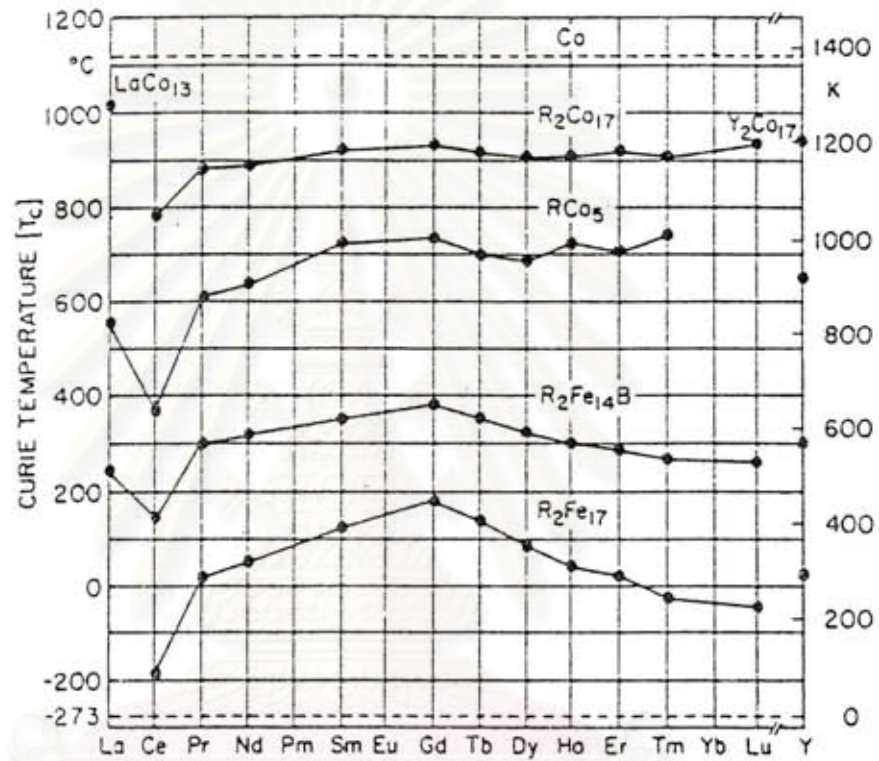


FIGURE 3.3 Curie Temperatures of the binary intermetallic RE-TM magnets.

(Data from Strnat, et al. 1991.)

สถาบันวิจัยบริการ  
จุฬาลงกรณ์มหาวิทยาลัย

### Insertion of H, C, or N in the RE-TM compounds

As pointed out,  $RE_2TM_{17}$  compounds are known to crystallize with either the rhombohedral  $Th_2Zn_{17}$  structure or the hexagonal  $Th_2Ni_{17}$  structure for light-RE and heavy-RE, respectively. Interest in this series has been renewed since it was shown that insertion of light interstitial atoms such as H, C, or N could raise the usually low Curie temperature of the ferromagnetic compounds as shown in Figure 3.4 (Isnard, Miraglia, Fruchart, Soubeyroux, et al., 1994).

For the rhombohedral structure, the hydrogen ion can enter into the octahedral 9e sites ( as shown in Figure 3.1a ), a full occupancy of these sites corresponds to 3 hydrogen atoms per formula unit. Other sites which might be available are the tetrahedral sites. Since it is known from repulsion criteria that the minimum H-H distance in hydrogenated intermetallic is 2.1 Å, this involves for the tetrahedral sites, a maximum occupancy of 1/3 (2 sites over 6) which corresponds to 2 hydrogen atoms per formula unit ( see Figure 3.5 ). So the maximum hydrogen amount that can be taken up is five (5) hydrogen atoms per formula unit. Such a maximum hydrogen concentration is observed for light-RE compounds while it goes down to 3 hydrogen atoms per formula unit for heavy-RE compounds. The filling of octahedral sites corresponds to a constant term in the hydrogenation induced volume expansion, whereas the filling of the tetrahedral sites would depend on the RE metal size. This is confirmed by neutron diffraction experiments (Kapsuta, et al., 1994 ; Yang et al., 1991), it was determined that for the  $RE_2Fe_{17}C_x$  and  $RE_2Fe_{17}N_x$  both C and N atoms occupy the octahedral 9e sites of the rhombohedral  $Th_2Zn_{17}$  structure and the maximum C and N content is 3 atoms per formula unit as shown in Figure (3.1a). The reason is that the Sm-Fe distance in  $Sm_2Fe_{17}N_x$  is found from extended X-ray-absorption fine structure (EXAFS) to be 2.502 Å, which localizes the nitrogen in the 9e sites. The 3b site is too close to the RE (2.07 Å) to accommodate the nitrogen (Otani et al., 1991). From geometrical and energetic consideration, the smaller atoms are merely held in the interstitial holes between the larger atoms. C or N atoms

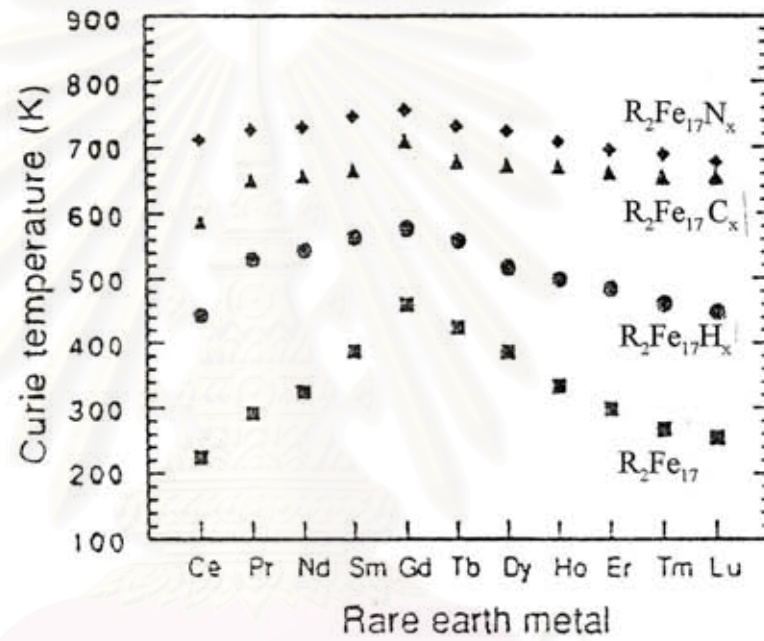


FIGURE 3.4 Curie Temperature of the ternary compounds formed by the absorption of H, C or N by the binary RE-TM compounds.

(Data from Isnard, Miraglia, Soubeyroux, et al. 1994.)

จุฬาลงกรณ์มหาวิทยาลัย



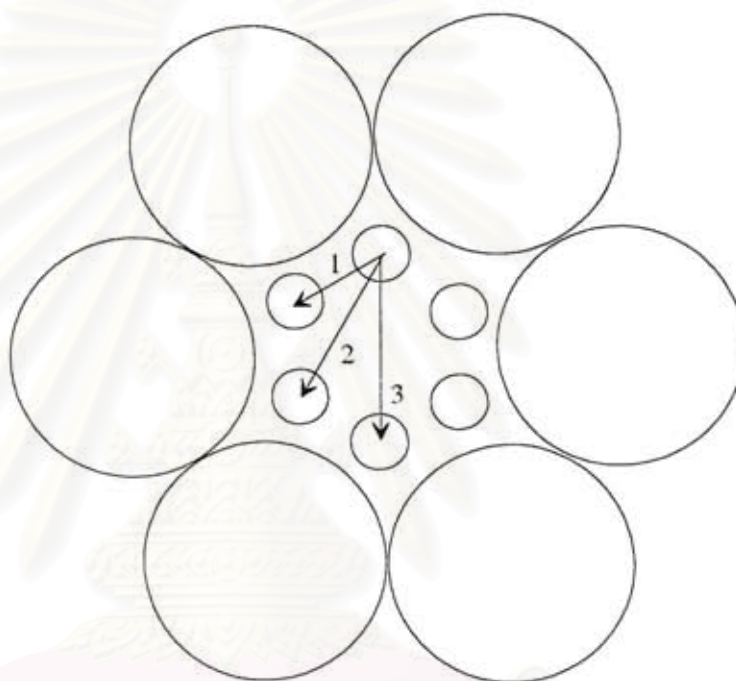


FIGURE 3.5  $\text{Th}_2\text{Zn}_{17}$  crystal structure showing the tetragonal sites into

which H ions can enter.

สถาบันวิทยบริการ  
จุฬาลงกรณ์มหาวิทยาลัย

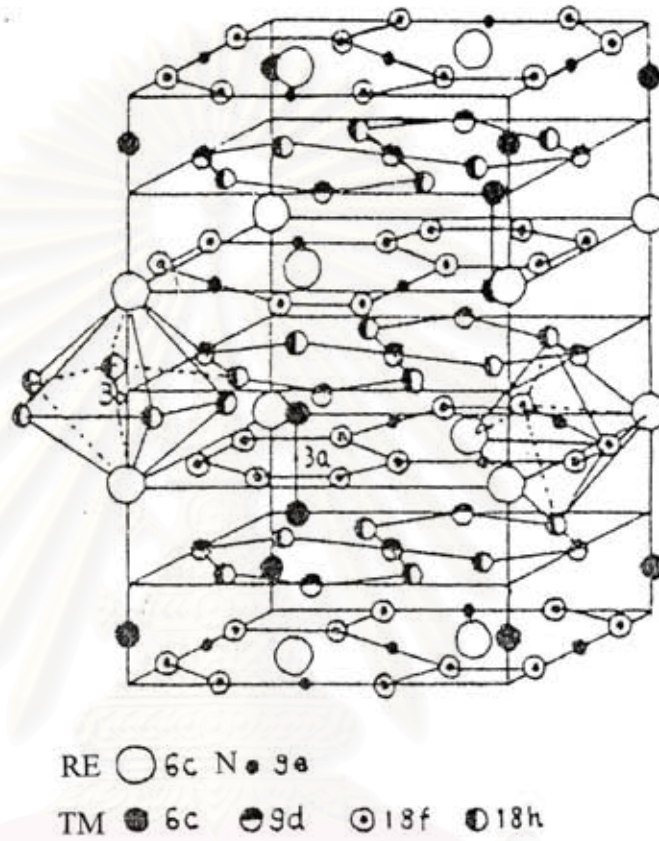


FIGURE 3.6 Schematic structure representation of  $\text{Nd}_2\text{Fe}_{17}\text{N}_3$ .

สถาบันวิทยบริการ  
 จุฬาลงกรณ์มหาวิทยาลัย

are inclined to occupy the largest volume interstitial sites, and avoid the smaller volume interstitial sites among all available interstices. Looking at Figure 3.6, we see that the 3a and 3b interstitial holes are too small to contain the N atom, whereas the 9e sites are large enough to hold a N atom. On the basis of this geometrical consideration, the 9e sites each N has two RE nearest neighbors.

#### Magnetic property of inserted RE-TM (C,H,N) compounds

The introduction of H, C or N atoms into  $RE_2TM_{17}$  compounds increases the molecular field coefficient  $\eta_{FF}$ , while  $\eta_{RR}$  and  $\eta_{RF}$  change slightly, with H, C or N concentration (Wang, Zhong, and Luo 1992), leading to an increase in the Curie temperature. To understand the  $T_c$  changes due to the H, C or N insertions at the microscopic level, we must remember that the Curie temperature of RE-TM intermetallic compounds depends mainly on the degree of localization of the 3d electrons in the TM atoms and on the distance between TM-TM atoms. The TM dumb-bell pairs in the  $Th_2Zn_{17}$  and  $Th_2Ni_{17}$  structures have a negative exchange interaction. This leads to the low mean value of TM-TM interaction energy and low Curie temperature of the  $RE_2Fe_{17}$  compounds. The insertion of C, H or N atoms to the RE-TM compounds lead to the lattice expansion. This expansion may reduce the negative exchange interactions of the TM dumb-bell pairs and may even make TM-TM exchange interactions positive.

สถาบันวิทยบริการ  
จุฬาลงกรณ์มหาวิทยาลัย

## CHAPTER IV



### EXPERIMENT DETAILS

In this chapter, we will discuss the experimental and measuring processes.

#### A. Nitrogenation

1. Powder of  $\text{Sm}_2\text{Co}_{17}$  alloys was obtained from Leico Industries, Inc. ( New York, U.S.A. ). Accurate amounts of this alloy was weighed on a Satorious Micro Balance belonging to the Department of Physics, Faculty of Science, Mahidol University. Many samples of  $\text{Sm}_2\text{Co}_{17}$  of about twenty (20) grams each were weighed out.

2. The powders were then heated and nitrogenated at various temperatures ( 300, 350 and 400° C ) for different time durations ( 1, 2, 3, 6 and 9 hours ) in the Linberg/Bluem Crucible Furnace ( Model 56724 ). Nitrogen gas flowed through the furnace at the rate of 0.3 CFH ( Cube feet per hour ). The furnace is shown in Figure 4.1.

3. The weight of each nitrogenated sample is taken and is compared with the mass of the sample before the nitrogenation. A relationship between the excess masses and the nitrogenated times at various temperatures is determined. The amount of nitrogen in moles in each nitrogenated sample is determined. Assume that the number of mole of nitrogen is not changed after nitrogenation, we can find out the value of  $x$  of each nitrogenated sample ( the calculation as shown in Appendix A ).

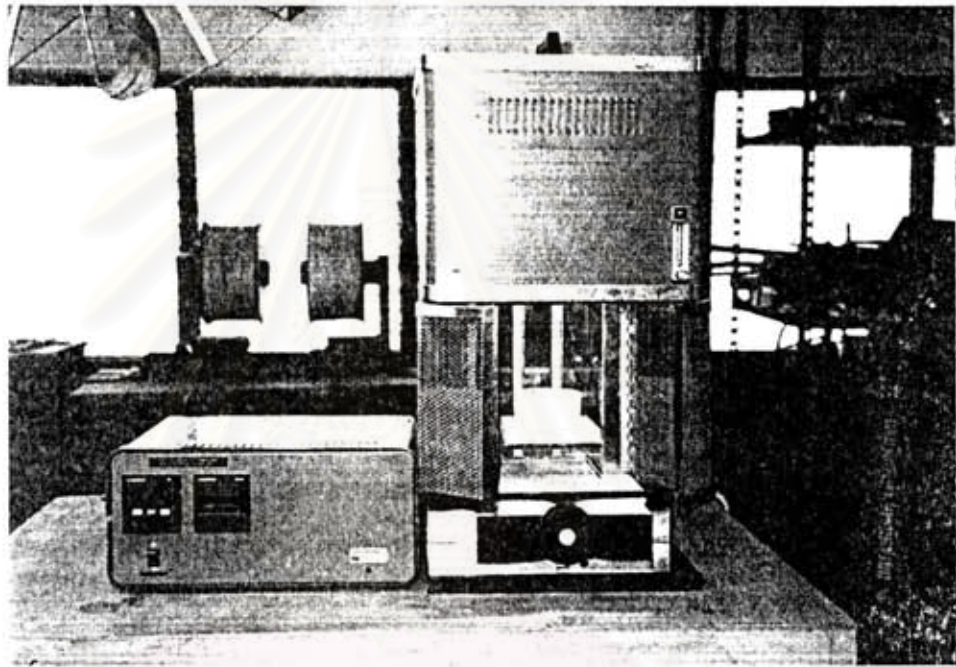


FIGURE 4.1 Linberg/Bluem 1700° C Crucible Furnace.

สถาบันวิทยบริการ  
จุฬาลงกรณ์มหาวิทยาลัย

## B. Characterization

1. The nitrogenated powders are analyzed by X-ray diffractometer (XRD) belonging to the Department of Geology, Faculty of Science, Chulalongkorn University. The Cu  $K\alpha$  line was used. From the XRD patterns, the lattice parameters (a,c) of the rhombohedral structure were determined by using a least square fit program ( which is given in Appendix B ).

2. The nitrogenated powder were reground using a pistil and mortar made from agate. An reflected light optical microscope ( belonging to the Department of Physics, Faculty of Science, Mahidol University ) was used to measure the particle sizes.

## C. Magnetic Property Measurements

1. Measurement of the magnetic properties required that the  $\text{Sm}_2\text{Co}_{17}$  powder be formed into circular pellets of 9 mm diameter for use in the Walker Scientific Magnetic Hysteresisgraph. This was done by mixing the ground powders with polyvinyl-alcohol ( 5% by weight in boiling water ). This is then put into the stainless steel mould, and pressed into a circular pellet by uniaxial press of about 500 lb/inch<sup>2</sup> for 1 minute.

2. Magnetic properties were measured with a Walker Scientific Hysteresis Graph model MH-10, MH-1020 shown in Figure 4.2. The hysteresisgraph belongs to the Department of Physics, Faculty of Science, Mahidol University. The hysteresis loop obtained can be used to determined the coercive force,  $H_c$ , the saturation magnetization,  $M_s$ , and the remanent magnetization,  $M_r$ . We can also find the relation between the magnetic properties and time of nitrogenation.

The results of these experiments will be discussed in the next chapter.



FIGURE 4.2 WALKER SCIENTIFIC MAGNETIC HYSTERESISGRAPH.

สถาบันวิทยบริการ  
จุฬาลงกรณ์มหาวิทยาลัย



## CHAPTER V

### RESULTS AND DISCUSSION

In this chapter we will consider the results of the measurements done in this research project. According to chapter IV, the experimental results can be classified into three categories. The first is the results from the nitrogenation process; the second, the characteristic of the samples and the third is the magnetic properties results.

#### A. Nitrogenation

As pointed out in Chapter IV, 20 gms of  $\text{Sm}_2\text{Co}_{17}$  powders for each of 5 different nitrogenated times at 3 different temperatures. Table 5.1 shows the masses before and after nitrogenated, and mole of nitrogen (x) entering into the  $\text{Sm}_2\text{Co}_{17}$  powder for each samples. Figures 5.1 and 5.2 show the relationship between percentage of nitrogen increased and mole of nitrogen, respectively, with the nitrogenated times.

The percent of nitrogen increases smoothly as the nitrogenated time increases ( below 6 hours ) and is almost constant at longer time ( above 9 hours ), and they also increase as the temperature increases. We suppose that during the nitrogenation, there are excess nitrogen to go through the  $\text{Sm}_2\text{Co}_{17}$  powders. Then we can calculate the number of moles of nitrogen (x) which are proportional to the percent of nitrogen increased. The maximum value of x is about 1.7, which is different from the other works.

Kattet et al. (Katter, Wecker, and Schultz, 1990) started from elemental Sm and Fe ( purity 99.5 and 99.9 %, respectively ).  $\text{Sm}_2\text{Fe}_{17}$  was first arc melted under an argon (Ar) atmosphere. Then the samples were wrapped in tantalum (Ta) foil and



sealed in Ar filled quartz tubes and held at 1440 K for 16 (h). The ground samples were nitrated in a Perkin-Elmer Thermo Gravimetric Analyser ( TGA 7 ) under a constant flow of nitrogen. The mass increase of 2.2 wt% after 15 h at 670 K led to a nominal formula of  $\text{Sm}_2\text{Fe}_{17}\text{N}_2$ . While Buschow et al. (Buschow et al, 1990), prepared by arc melting the elemental Sm and Fe. After that the samples were vacuum annealed at temperatures between 900 and 1000 ° C for about 10 days. And then the annealed samples were heated in an atmosphere of purified nitrogen gas for about 3 h at 500 ° C. The composition of the compounds corresponded to the formula composition  $\text{R}_2\text{Fe}_{17}\text{N}_{2.5}$  ( R is the rare-earth ). Another group, Isnard et al. (Isnard, Miraglia, Fruchart, and Guillot, 1994) prepared the alloy by induction melting in a cold crucible under an Ar atmosphere. They used a solid-gas reaction to prepare the insertion compounds where the starting samples was ground into a fine powder. They used nitrogen gas at typical reaction temperatures between 450 and 550 ° C. The largest nitrogen concentration that could be accommodated in these compounds is 3N atoms per formula unit. In our method, we used  $\text{Sm}_2\text{Co}_{17}$  powder obtained from Leico Industries, Inc. ( New York, U.S.A.) and then heated and nitrogenated in the Linberg/Bluem Crucible Furnace ( Model 56724 ) by flowing nitrogen gas through the furnace at the rate of 0.3 CFH. The nitrogen that can diffuse into structure may not reach the maximum amount possible due to the lower temperature and shorter time used. Our working temperatures are more reasonable than our nitrogenation time, as we can see from Figures 5.1 and 5.2.

สถาบันวิทยบริการ  
จุฬาลงกรณ์มหาวิทยาลัย

TABLE 5.1

Mass of samples before and after nitrogenation

Nitrified		Weights of $\text{Sm}_2\text{Co}_{17}$ [gms]			Nitrogen% increase	Mol of Nitrogen
Temp. [°C]	Time [h]	Before	After	Nitrogen		
300	1	20.1164	20.1637	0.0473	0.2351	0.2187
	2	20.0629	20.1331	0.0701	0.3494	0.3249
	3	20.1629	20.2535	0.0906	0.4493	0.4179
	6	20.0342	20.1556	0.1214	0.6061	0.5636
	9	20.0552	20.1963	0.1411	0.7036	0.6543
350	1	20.2187	20.3569	0.1382	0.6835	0.6357
	2	20.1605	20.3256	0.1651	0.8189	0.7616
	3	20.0462	20.2255	0.1793	0.8944	0.8318
	6	20.0463	20.2702	0.2239	1.1169	1.0387
	9	20.0558	20.3049	0.2491	1.2421	1.1551
400	1	20.1367	20.3433	0.2066	1.0261	0.9542
	2	20.186	20.4353	0.2493	1.2351	1.1486
	3	20.1934	20.4764	0.2831	1.4014	1.3034
	6	20.0577	20.3898	0.3321	1.6557	1.5398
	9	20.1837	20.5494	0.3657	1.8119	1.6851

จุฬาลงกรณ์มหาวิทยาลัย

## The Relation of SmCo (2-17) between Nitriding Time & Nitrogen % increase

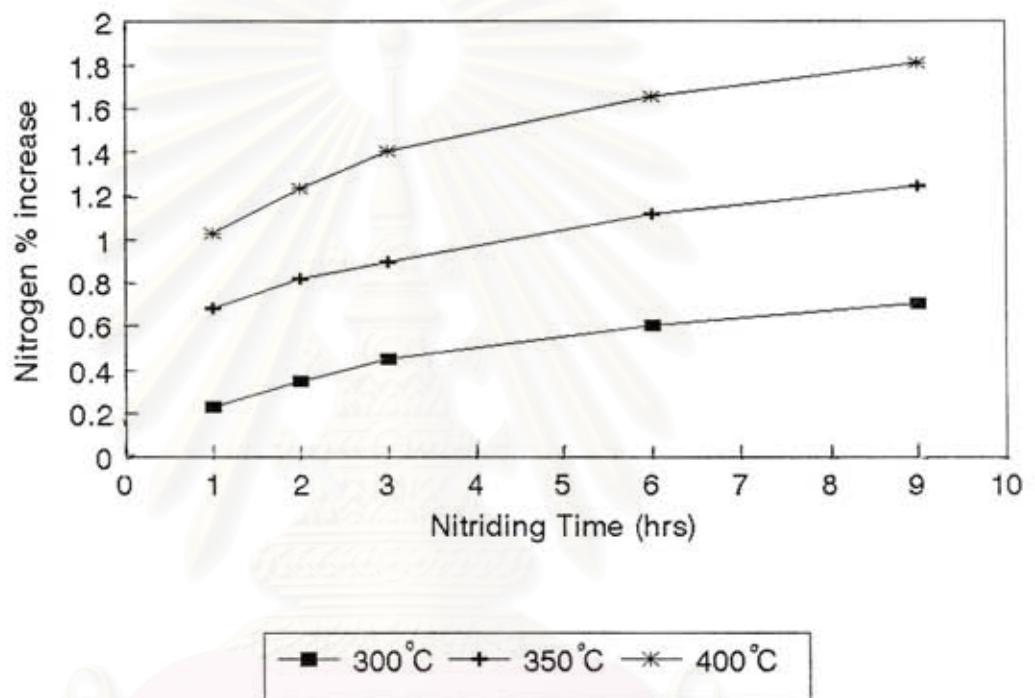


FIGURE 5.1 Percentage weight of nitrogen absorbed as a function of  
nitrogenating time.

สถาบันวิทยบริการ  
จุฬาลงกรณ์มหาวิทยาลัย

## The Relation of SmCo (2-17) between Nitriding Time & Mol of Nitrogen

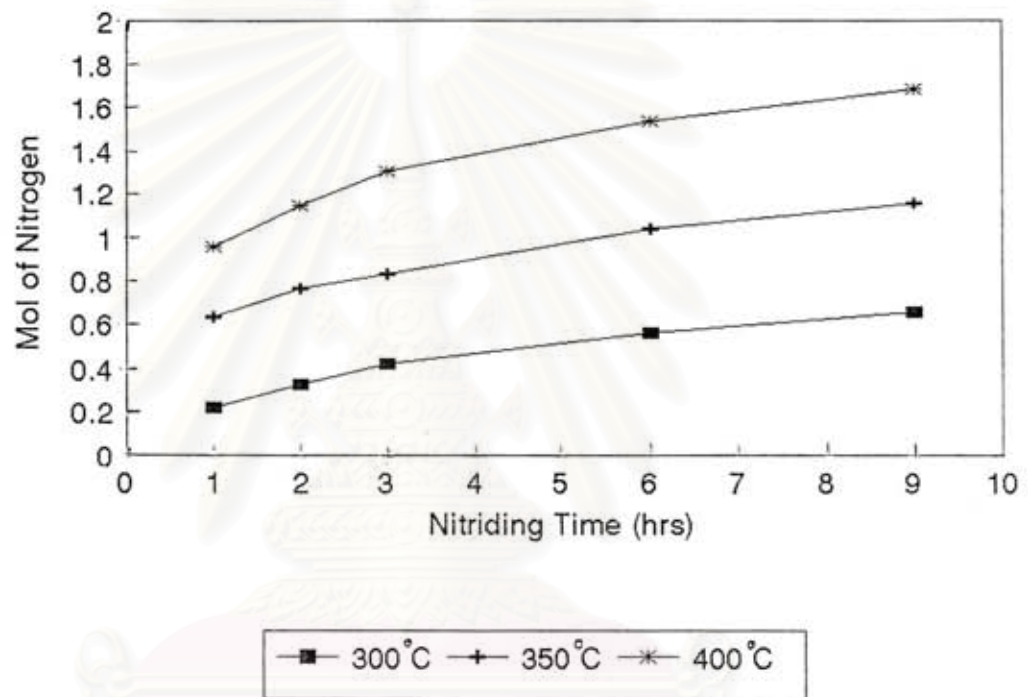


FIGURE 5.2 Mole fraction of nitrogen absorbed as a function of nitrogenating time.

## B. Sample Characterization

### i. Lattice parameters

The lattice parameters (  $a, c$  ) for the  $\text{Sm}_2\text{Co}_{17}\text{N}_x$  were calculated using the XRD patterns taken ( a typical XRD pattern is shown on Figure 5.3 ) and identifying the relevant Miller indices from the table of  $\text{Sm}_2\text{Co}_{17}$  with  $\text{Th}_2\text{Zn}_{17}$  rhombohedral structure ( shown in Appendix A ). Table 5.2 and Figure 5.4 show the  $a, c$  parameters for various  $\text{Sm}_2\text{Co}_{17}\text{N}_x$  powders.

As we see, the lattice parameter  $a$  increases with nitrogenation time while lattice parameter  $c$  is decreased after nitrogenation. This shows that the nitrogen has diffused into the  $\text{Sm}_2\text{Co}_{17}$  structure and occupies some sites in the structure. Occupation of the interstitial sites in the  $ab$  plane causes the expansion along  $a$ -axis. The contraction along  $c$ -axis is probably due to the increase in the density of the samples during the nitrogenation.

### ii. Particle sizes

The ground powders sizes were measured with a reflected light microscope. The particle sizes were about 5-10 microns. The change in the particle sizes are listed in Table 5.3. Their shapes have sharp edges at each corners. Some big grains were made up of many smaller ones. Several photographs of the grains are shown in Figure 5.5.

สถาบันวิทยบริการ  
จุฬาลงกรณ์มหาวิทยาลัย

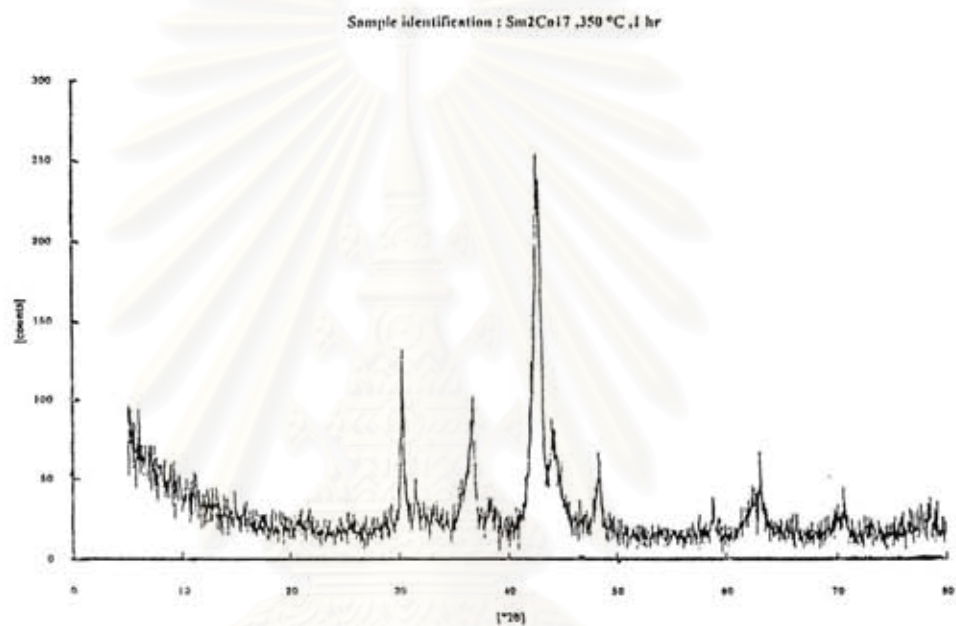


FIGURE 5.3 A typical XRD pattern for Sm<sub>2</sub>Co<sub>17</sub>N<sub>x</sub>.

สถาบันวิทยบริการ  
จุฬาลงกรณ์มหาวิทยาลัย

TABLE 5.2

Lattice parameters ( a, c ) changes as  
a function of nitrogenating time

Nitrified		Lattice parameters		
Temp.[°C]	Time [h]	a [°A]	c [°A]	c/a
300	1	8.4472	12.2562	1.4509
	2	8.4557	12.2309	1.4465
	3	8.4451	12.2803	1.4541
	6	8.4430	12.2662	1.4528
	9	8.4462	12.2618	1.4518
350	1	8.4552	12.2588	1.4499
	2	8.4526	12.2578	1.4502
	3	8.4502	12.2654	1.4515
	6	8.4477	12.2846	1.4542
	9	8.4443	12.2669	1.4527
400	1	8.4429	12.2553	1.4516
	2	8.4472	12.2686	1.4524
	3	8.4475	12.2671	1.4522
	6	8.4520	12.2623	1.4508
	9	8.4426	12.2733	1.4537
Before Nitrified		8.4412	12.2914	1.4561
Data from Table		8.4020	12.1720	1.4487
Cal. from Table		8.3951	12.1846	1.4514

\*\*\* Use 5 highest peaks [113], [300],[220],[303],[214]

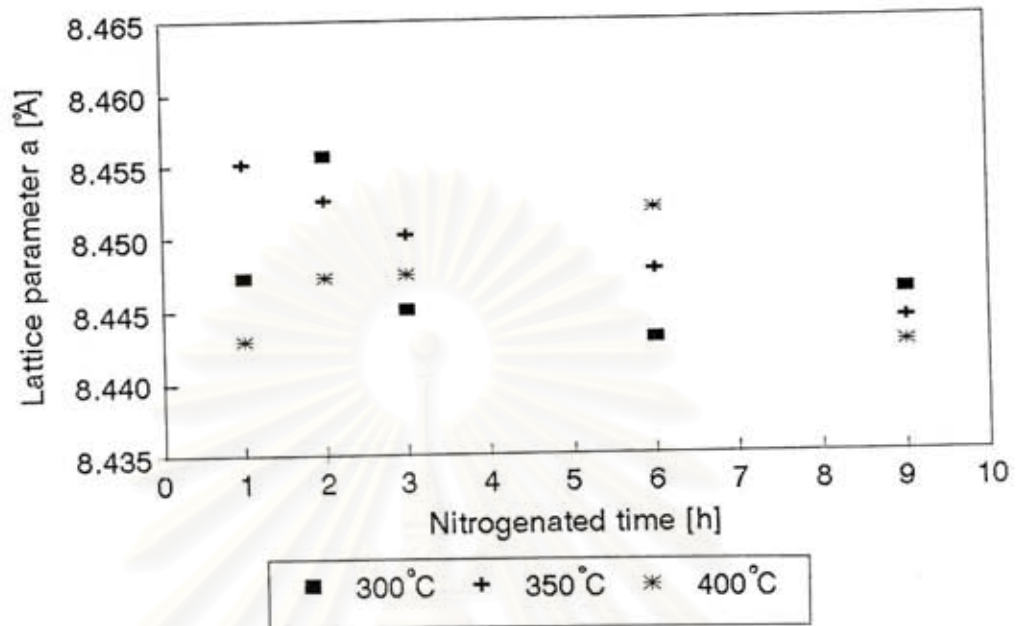


Figure 5.4a.

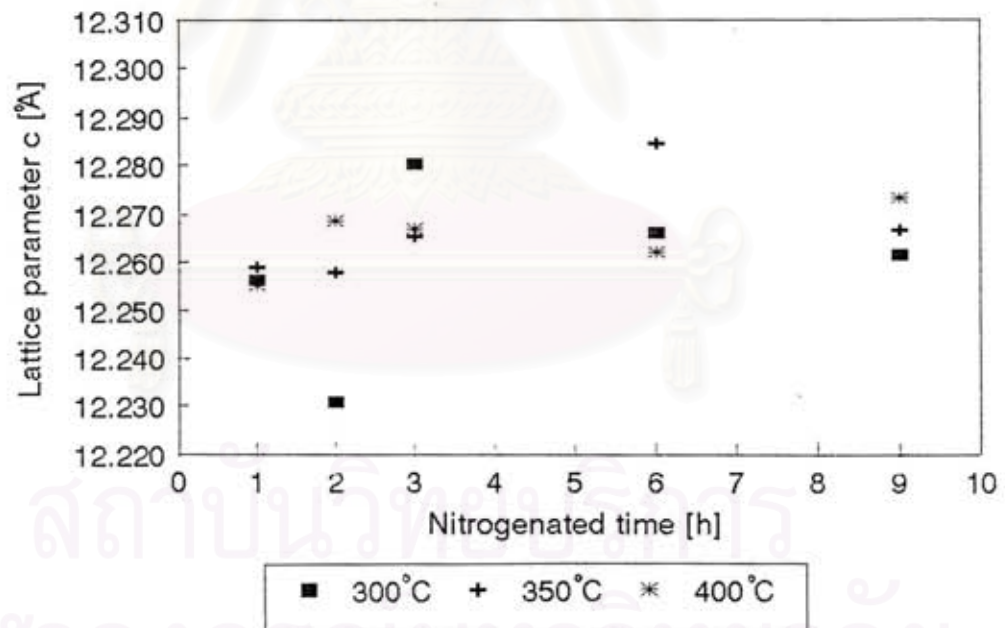


Figure 5.4b.

FIGURE 5.4 Changes in the Lattice Parameters as a function of nitrogenation time. (5.4a) parameter- $a$ , (5.4b) parameter- $c$ .



TABLE 5.3

Particle ( grain ) sizes for specimens nitrogenated for different time durations and temperatures.

Nitrided		Particle size
Temp.[°C]	Time [h]	[micron]
300	1	11.975
	2	7.200
	3	9.048
	6	10.819
	9	5.829
350	1	7.286
	2	6.000
	3	8.000
	6	7.937
	9	7.175
400	1	9.922
	2	9.143
	3	7.143
	6	7.600
	9	9.086

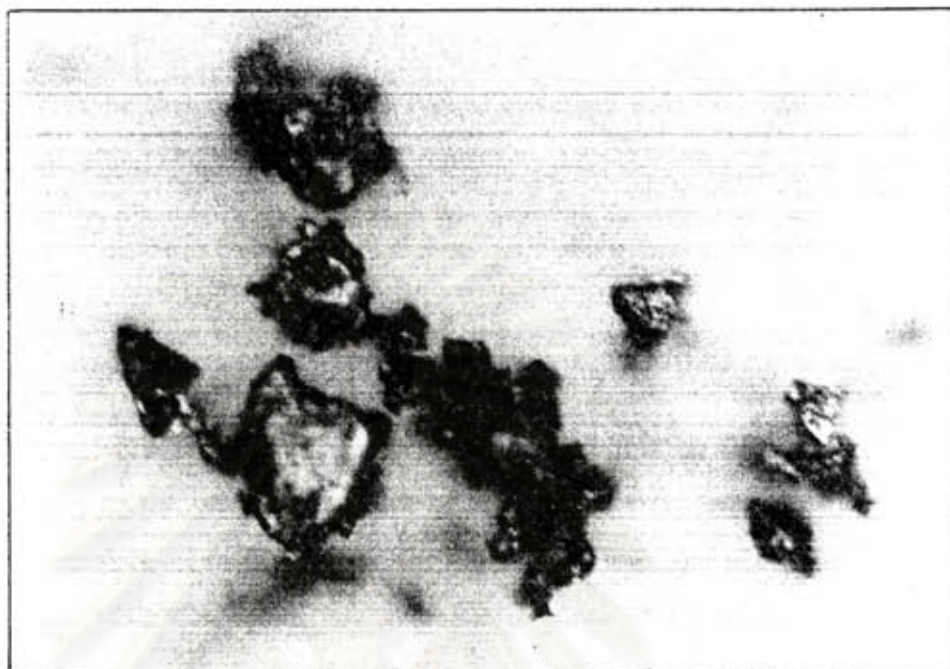


Figure 5.5a.

10  $\mu\text{m}$ 

Figure 5.5b.

10  $\mu\text{m}$ 

FIGURE 5.5 Photographs of the grains used to determine grain sizes.

( 5.5a )  $\text{Sm}_2\text{Co}_{17}\text{N}_x$  at 400 °C for 6 hours [ 720x ]

( 5.5b )  $\text{Sm}_2\text{Co}_{17}\text{N}_x$  at 300 °C for 9 hours [ 720x ]

### C. Magnetic Properties

From the hysteresis graphs ( a typical hysteresis loop is shown on Figure 5.6 ), the saturation magnetization  $M_s$ , the remanent magnetization  $M_r$ , the coercivity  $H_c$  and the energy product  $(BH)_{max}$  for each specimen can be obtained.

#### i. Saturation magnetization $M_s$

As we see from Table 5.4 and Figure 5.7, the saturation magnetizations increase with nitrogenation time ( except for the nine hour specimens ). This increase in  $M_s$  is due to the increased amount of nitrogen entering into the interstitial sites. Since the amounts of magnetic ions, the Co and Sm ions, are not changing and since nitrogen ion does not possess any magnetic moment, the increase in the saturation magnetization must be due to changes in the exchange interactions. To see how this can occur, we note first that insertion of nitrogen causes an increase in the Curie temperature. Looking at eqn. 2.1, we see that an increase in the TM-TM interaction would also cause an increase in the Curie temperature. At the end of Chapter III, we have given a brief discussion of how N, C or H insertion could cause an increase in the TM-TM interaction. Carrying the logic one step further, the local field ( given by eqn. 2.5 ) acting on a TM ion in the Sm-Co system would also become bigger if the TM-TM interaction increased. Insertion of the larger local field into eqn. 2.7 would give an increased magnetization of the TM sublattice for two reasons. The beginning of the saturation would begin at a high temperature due to the increased local field and secondly, the relative temperature entering into the temperature dependent magnetization,  $T_{RoomT}/T_c$  (  $T_{RoomT}$  being the temperature at which the measurements were taken ) would be smaller since  $T_c$  would be higher.

จุฬาลงกรณ์มหาวิทยาลัย

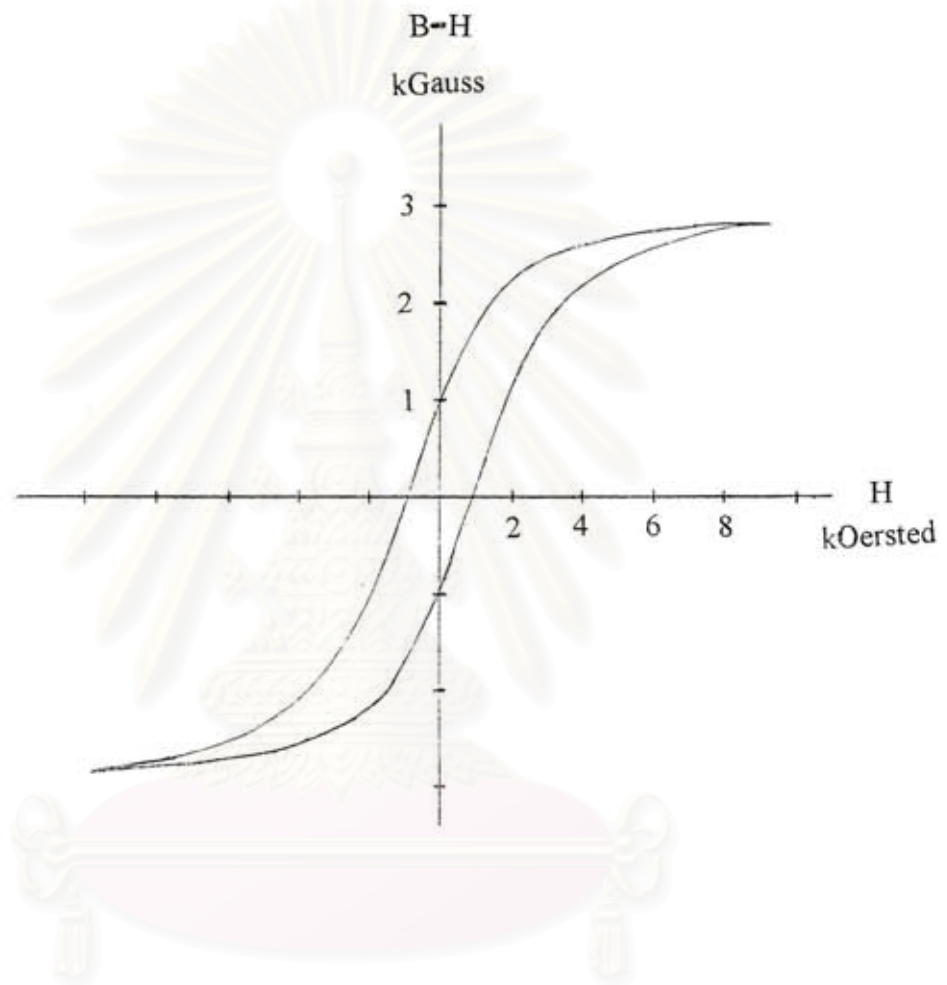


FIGURE 5.6 Hysteresis Loop of a typical  $\text{Sm}_2\text{Co}_{17}\text{N}_x$  specimen.

สถาบันวิทยบริการ  
จุฬาลงกรณ์มหาวิทยาลัย

TABLE 5.4  
Magnetic Properties of  $\text{Sm}_2\text{Co}_{17}\text{N}_x$

Nitrided		$H_c$	$4\pi M_s$	$4\pi M_r$
Temp. [ °C ]	Time [ h ]	[ Oersted ]	[ Gauss ]	[ Gauss ]
300	1	1370.00	2525.00	1100.00
	2	1300.00	2233.33	933.33
	3	1100.00	2387.50	975.00
	6	1100.00	2300.00	850.00
	9	1050.00	2287.50	825.00
350	1	1150.00	2616.67	1100.00
	2	750.00	2400.00	950.00
	3	800.00	2800.00	1000.00
	6	900.00	2650.00	900.00
	9	1000.00	2325.00	887.50
400	1	1100.00	2100.00	912.50
	2	950.00	1725.00	866.75
	3	1050.00	1975.00	812.50
	6	1000.00	2000.00	800.00
	9	900.00	2191.67	687.50

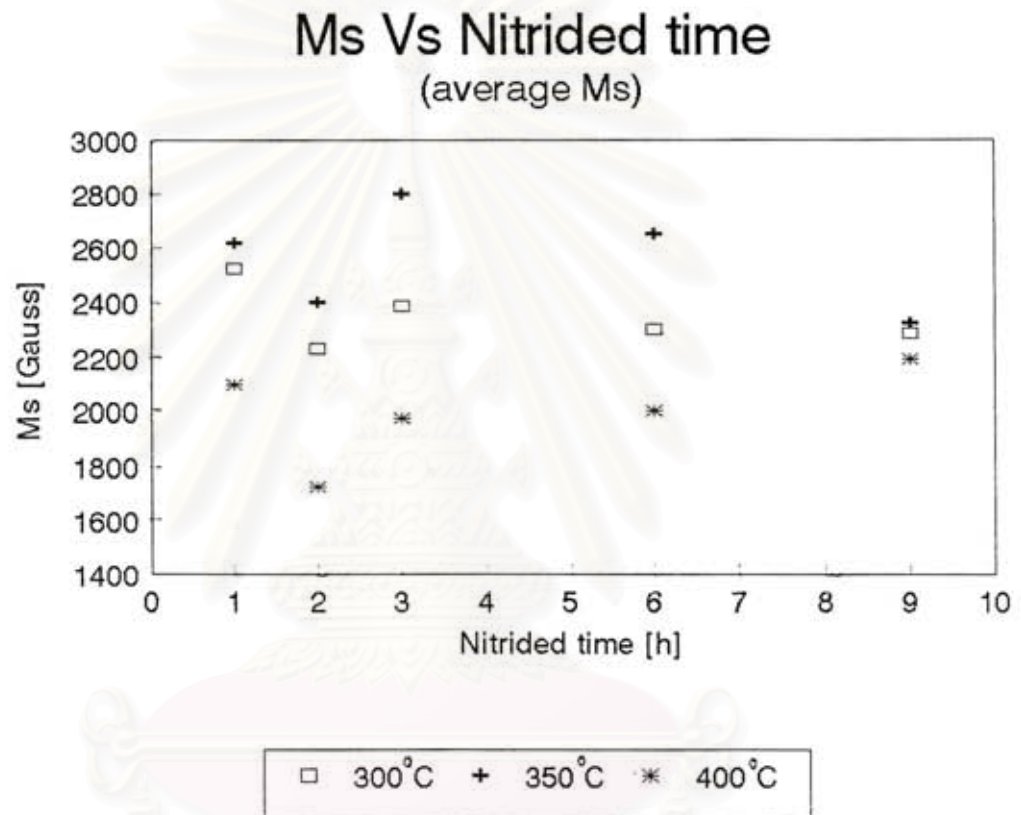


FIGURE 5.7 Saturation magnetization of  $\text{Sm}_2\text{Co}_{17}\text{N}_x$  specimens as a function of nitrogenation time.

สถาบันวิจัยบริการ  
จุฬาลงกรณ์มหาวิทยาลัย

### ii. Remanent Magnetization

The remanent magnetizations of the  $\text{Sm}_2\text{Co}_{17}\text{N}_x$ , nitrogenated for different time intervals are shown on Figure 5.8. We see in general that for a given duration of time, the remanent magnetization of the higher processed specimen have the higher values. Also the remanent magnetization decreases with increasing nitrogenation time.

### iii. Coercive Force

On Figure 5.9, the coercive force of  $\text{Sm}_2\text{Co}_{17}\text{N}_x$  is plotted as a function of the nitrogenation time for various processing temperatures. As is seen, the coercive force decreases when the processing temperature is increased. It increases as the duration time of the nitrogenation increases. Looking at Table 5.5, the coercive force of most magnetic compounds is not depend on the grain size and the behavior seen in here is different from what is usually seen.

### iv. $(\text{BH})_{\text{max}}$ of $\text{Sm}_2\text{Co}_{17}\text{N}_x$

Using the information obtained from the hysteresis loops ( demagnetization curve, second quadrant of the hysteresis curve ), the energy products (BH) are calculated for different B's ( see Figure 5.10 ). The maximum energy product  $(\text{BH})_{\text{max}}$  is the value where the tangent to the curve is infinity. The maximum energy products for the different  $\text{Sm}_2\text{Co}_{17}\text{N}_x$  are listed in Table 5.6. The highest value is 0.24 MGOe ( 1.91 J/m<sup>3</sup> ) for nitriding at 300 °C for 2 h. This is the energy stored in the sample after removing the applied field.

สถาบันวิทยบริการ  
จุฬาลงกรณ์มหาวิทยาลัย

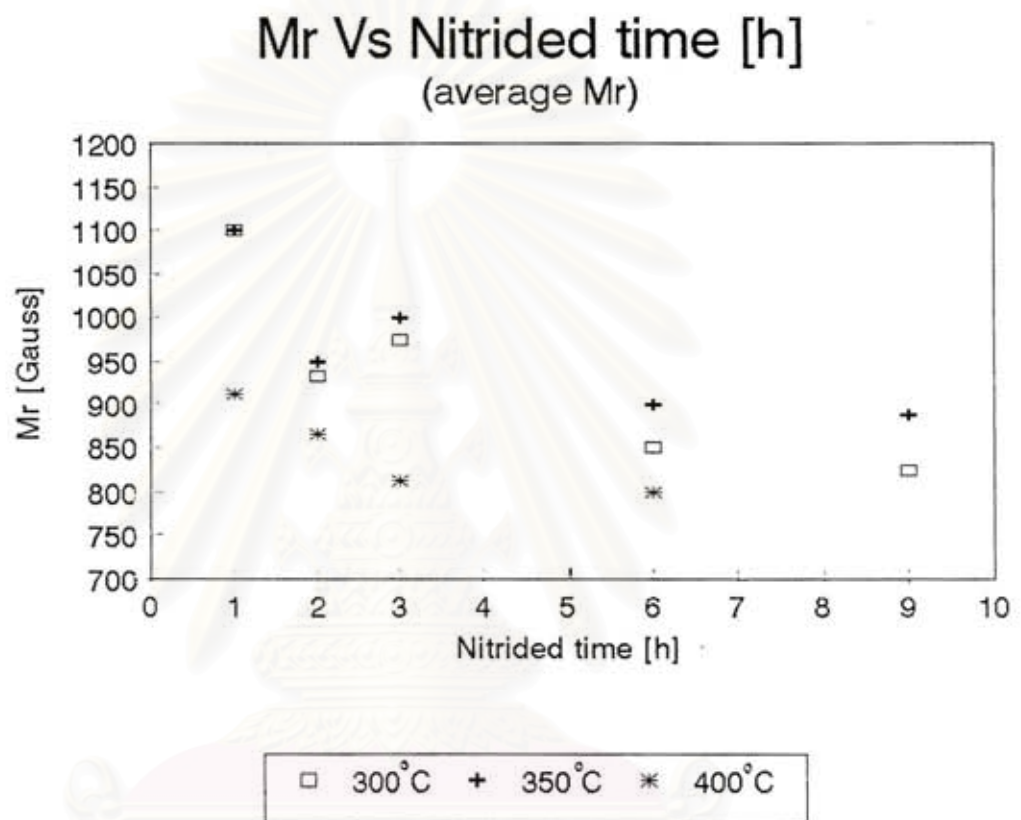


FIGURE 5.8 Remanent magnetization of  $\text{Sm}_2\text{Co}_{17}\text{N}_x$  specimens as a function of nitrogenation time for various processing temperatures.

สถาบันวิทยบริการ  
จุฬาลงกรณ์มหาวิทยาลัย



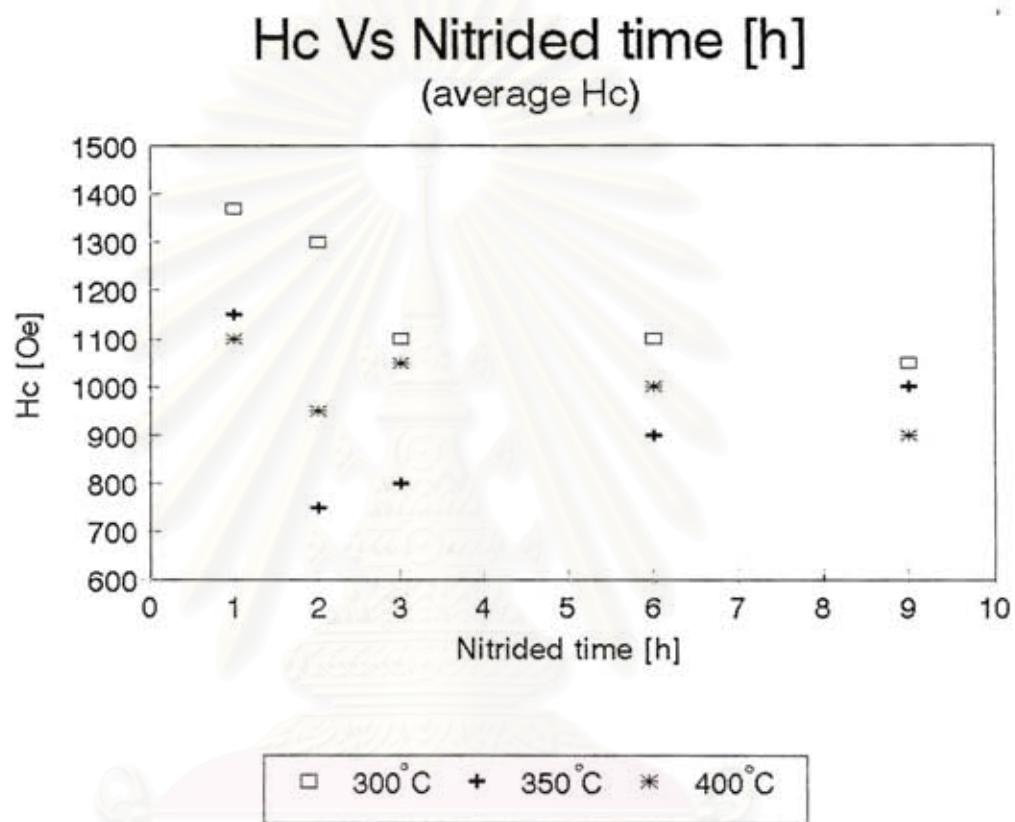


FIGURE 5.9 Coercive Force of  $\text{Sm}_2\text{Co}_{17}\text{N}_x$  specimens as a function of nitrogenation time for various processing temperatures.

สถาบันวิทยบริการ  
จุฬาลงกรณ์มหาวิทยาลัย

TABLE 5.5

The relationship between the coercive force ( $H_c$ ) and particle sizes

Nitrided		$H_c$ [ Oersted ]	Particle sizes [ $\mu\text{m}$ ]
Temp.[ $^{\circ}\text{C}$ ]	Time [h]		
300	1	1370.00	11.975
	2	1300.00	7.200
	3	1100.00	9.048
	6	1100.00	10.819
	9	1050.00	5.829
350	1	1150.00	7.286
	2	750.00	6.000
	3	800.00	8.000
	6	900.00	7.937
	9	1000.00	7.175
400	1	1100.00	9.922
	2	950.00	9.143
	3	1050.00	7.143
	6	1000.00	7.600
	9	950.00	9.086

สถาบันวิทยบริการ  
จุฬาลงกรณ์มหาวิทยาลัย

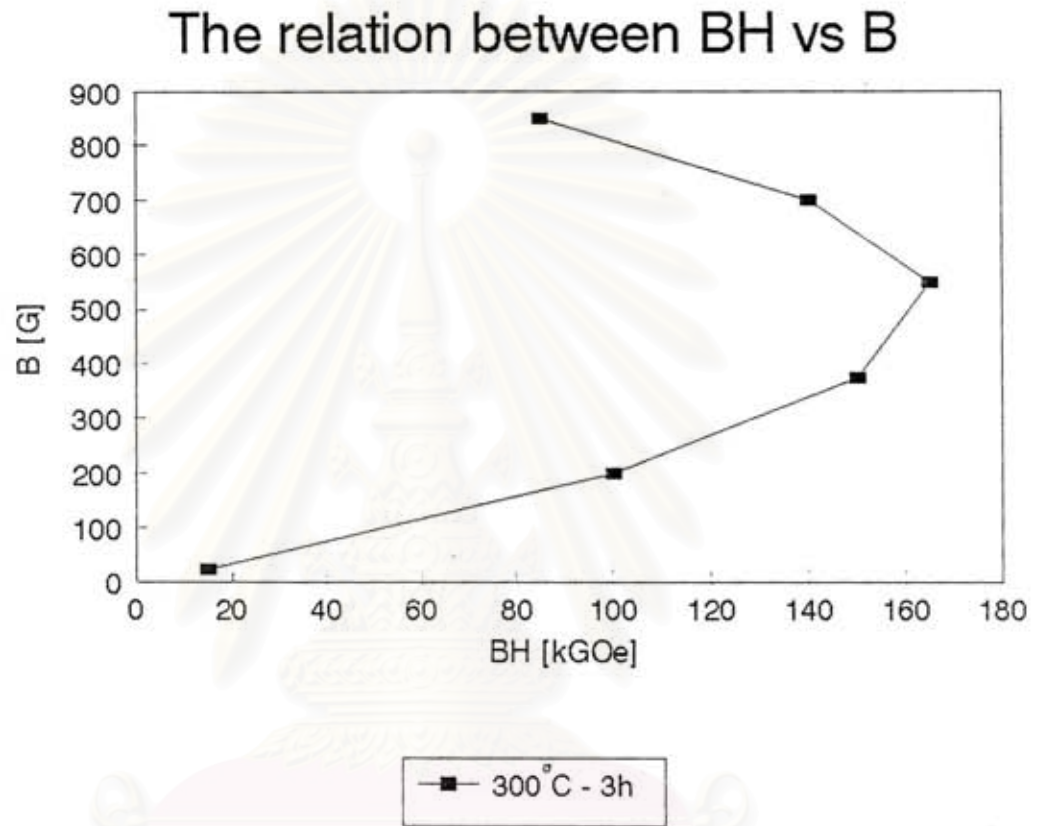


FIGURE 5.10 A plot of the energy product BH for different values of B of a typical  $\text{Sm}_2\text{Co}_{17}\text{N}_x$  magnet.

สถาบันวิทยบริการ  
จุฬาลงกรณ์มหาวิทยาลัย

TABLE 5.6

 $(BH)_{\max}$  of the nitrated  $\text{Sm}_2\text{Co}_{17}$ 

Nitrated		$B=H+4\pi M$	$(BH)_{\max}$	$(BH)_{\max}$
Temp. [°C]	Time [h]	Gauss	kGOe	J/m <sup>3</sup>
300	1	525.00	210.00	1.67
	2	600.00	240.00	1.91
	3	725.00	217.50	1.73
	6	675.00	202.50	1.61
	9	475.00	142.50	1.13
350	1	650.00	195.00	1.55
	3	500.00	150.00	1.19
	6	400.00	120.00	0.96
	9	450.00	135.00	1.07
400	1	525.00	210.00	1.67
	2	650.00	130.00	1.03
	3	375.00	112.50	0.90
	6	750.00	150.00	1.19
	9	375.00	112.50	0.90

[ 1 GOe =  $79.58 \times 10^4$  J/m<sup>3</sup> ]

สถาบันวิจัยบริการ  
จุฬาลงกรณ์มหาวิทยาลัย

## CHAPTER VI



## CONCLUSION

This study represents a preliminary investigation of the effects of nitrogenation of  $\text{Sm}_2\text{Co}_{17}$  magnets. As pointed out in the Chapter II, the nitrogenation of the 2-17 magnets was done in order to raise the Curie temperatures of  $\text{Sm}_2\text{Fe}_{17}$  magnets to far above the ambient temperatures at which the magnets operate. The Curie temperatures of  $\text{Sm}_2\text{Co}_{17}$  are already above these temperatures but because of the higher cost of cobalt, ways to increase the Curie temperatures of Fe-based magnets were sought. The techniques used to raise the temperature were accompanied by other changes. The object of the present study was to see if these other changes still occurred when the nitrogenation is applied to the Co-based magnets.

### i. Nitrogenation

Looking at Table 5.1, we see that increasing the nitrogenation temperature has a greater effect on the amount of nitrogen being absorbed than does the duration of the nitrogenation for short times. The diffusion constant should be a function of temperature and the behavior that we see reflects this. Since the percentage of increase is still climbing for all nitrogenation temperatures, a uniform distribution of the nitrogen among all the interstitial sites within the structure has not been achieved. Most of the scattering seen in the data appearing in most Figures may be due to the nonhomogeneity of the specimens.

### ii. Saturation Magnetization

Because of the nonhomogeneity of the specimens, the value of the saturation magnetization are very low and nearly constant for the 400 °C and the 300 °C series ( except the 2 h data ), while the 350 °C series intend to decrease for the longer of

nitrogenation time ( see Figure 5.7 ), which is contrasted with the theory. From the theory, when nitrogen atoms go into the crystal lattice, the volume is expanded. So the interaction between the Co-Co atoms should be increased, and the saturation magnetization should be increased too.

### iii. Coercive Force

The coercivity remains low ( see Figure 5.9 ), unlike the other works. Table 6.1 shows the comparison of the magnetic properties for each group. We can see that most of the other works have higher magnetic properties than our results. The reason may be that the coercivity is however dependent on the processing conditions. This may be a direction for future studies.

### iv. Remanent Magnetization

The remanent magnetization, Table 5.4, is decreased from the value of 1100 to 800 Gauss, which is very small compared to  $M_r$  ( $M_r \ll 0.5 M_s$ ). And it is also very low comparing with the other results. By increasing the coercivity, the hysteresis loop might be made more square so that the remanent magnetization approaches the value of the saturation magnetization. This means that in the future, more attention should be paid to the processing conditions.

### v. Energy Product

The energy product is very much lower than the other works. Our highest value is 0.24 MGOe obtained from nitriding at 300 °C for 2 h. This may be that our samples have not been magnetized so they are not reach the saturation states. We can also see that the  $(BH)_{max}$  decreases as the nitrogenation time increases. This means that for the longer time of nitrogenation, the nitrogen may be come out of the crystal.

From this study, the experimental results are unlike the others. It may be that our sample ( $Sm_2Co_{17}$  from the Leico Industries, Inc.) has some impurities, due to the preparation process, which may reduce some magnetic properties ( $M_r$  and  $M_s$ ). The coercivity is still low due to the powder sizes which are not uniform. Furthermore the

nitrogenation process does not reach the equilibrium ( because of the shorter time and lower temperature ) that make the specimen be inhomogeneous. These may be the reasons why our magnetic properties are very low comparing with the others. To improve these properties we should pay more attention to the preparation and nitrogenation process, so that the single phase of  $\text{Sm}_2\text{Co}_{17}$  and the homogeneity of the specimen should be obtained.

TABLE 6.1

Comparison of the magnetic properties

Sample	$H_c$ [ kOe ]	$M_r$ [ kG ]	$(BH)_{max}$ [ MGOe ]
A	6.6	9.4	18.0
B	1-4	12.5	39.0
C	23.5	11.3	30.1
D	1.4	1.1	0.24

A is  $\text{Sm}_2\text{Co}_{17}$  produces by Kneller et al. 1991.

B is  $\text{Sm}_2\text{Co}_{17}$  produces by Strnat, K.J. and Strnat, R.M.W. 1991.

C is  $\text{Sm}_2\text{Co}_{17}$  produces by Hasegawa et al. 1993.

D is  $\text{Sm}_2\text{Co}_{17} \text{N}_x$  obtained in this thesis.



## REFERENCES

- Altounian, Z., Chen, X., Liao, L.X., Ryan, D.H., and Strom-Olsen, J.O. 1993. J. Appl. Phys. 73 (10) : 6017-6022.
- Ballou, R. 1994. The role of R-M compounds in the understanding of magnetism. J. Magn. Magn. Mater. 129 : 1-9.
- Buschow, K.H.J., Coehoorn, R., de Mooij, D.B., de Waard, K., and Jabobs, T.H. 1990. Structure and magnetic properties of  $R_2Fe_{17}N_x$  compounds. J. Magn. Magn. Mater. 92 : L35-L38.
- Duc, N.H., Hien, T.D., Givord, D., Franse, J.J.M., and de Boer, F.R. 1993. Exchange interactions in rare earth-transition metal compounds. J. Magn. Magn. Mater. 124 : 305-311.
- Hasegawa, M., Uchida, K., Nozawa, Y., Endoh, M., Tanigawa, S., Sankar, S.G., and Tokunaga, M. 1993. J. Magn. Magn. Mater. 124 : 325-329.
- Isnard, O., Miraglia, S., Fruchart, D., and Guillot, M. 1994. High field magnetization measurements of  $Sm_2Fe_{17}$ ,  $Sm_2Fe_{17}N_3$ ,  $Sm_2Fe_{17}D_5$ , and  $Pr_2Fe_{17}$ ,  $Pr_2Fe_{17}N_3$  (invited). J. Appl. Phys. 75 (10) : 5988-5993.
- \_\_\_\_\_. Miraglia, S., Soubeyroux, J.L., Fruchart, D., and l'Heritier, P. 1994. A structural analysis and some magnetic properties of the  $R_2Fe_{17}H_x$  series. J. Magn. Magn. Mater. 137: 151-156.
- Jiles, D. 1991. Introduction to Magnetism and Magnetic materials. 1st ed. London : Chapman & Hall.
- Kapusta. Cz., Rosenberg, M., Riedi, P.C., Datter, M., and Schultz, L. 1994. Nuclear magnetic resonance study of the  $Sm_2Fe_{17}N_x$  compounds. J. Magn. Magn. Mater. 134 : 106-112.



- Katter, M., Wecker, J., and Schultz, L. 1990. Magnetocrystalline anisotropy of  $\text{Sm}_2\text{Fe}_{17}\text{N}_2$ . J. Magn. Magn. Mater. 92 : L14-L18.
- Kneller, E.F., and Hawig, R. 1991. IEEE Trans. Magn. 27 : 3588.
- Kou, X.C., Grossinger, R., Katter, M., Wecker, J., Schultz, L., Jacobs, T.H., and Buschow, K.H.J. 1991. J. Appl. Phys. 70 (4) : 2272-2281.
- Otani, Y., Hurley, D.P.F., Sun, H., and Coey, J.M.D. 1991. Magnetic properties of a new family of ternary rare-earth iron nitrides  $\text{R}_2\text{Fe}_{17}\text{N}_{3.5}$  ( invited ). J. Appl. Phys. 69 (8) : 5584-5589.
- Parker, R.J. 1990. Advances in permanent magnetism. New York : John Wiley & Sons.
- Smith, W.F. 1993. Foundations of materials sciences and engineering. 2nd ed. New York : McGraw-Hill.
- Strnat, K.J., and Strnat, R.M.W. 1991. Rare earth-cobalt permanent magnets. J. Magn. Magn. Mater. 100 : 38-56.
- Wang, Q., Zhong, X.P., and Luo, H.L. 1992. Molecular field theory analysis of  $\text{R}_2\text{Fe}_{17}\text{C}_x$  ( R = Sm, Er ) compounds. J. Magn. Magn. Mater. 110 : 170-174.
- Yang, Y.C., Zhang, X.D., Kong, L.S., and Pan, Q. 1991. Neutron diffraction study of ternary nitrides of the type  $\text{R}_2\text{Fe}_{17}\text{N}_x$ . J. Appl. Phys. 70 (10) : 6018-6020.

สถาบันวิทยบริการ  
จุฬาลงกรณ์มหาวิทยาลัย

## APPENDIX A

### CALCULATION OF THE NUMBER OF MOLE OF NITROGEN IN THE NITRIDED COMPOUNDS

To calculate the number of mole of nitrogen, we first assume that the number of mole of  $\text{Sm}_2\text{Co}_{17}$  is not changed after nitrogenation. The weight of  $\text{Sm}_2\text{Co}_{17}$  is 1302.66 gms ( Sm = 150.4 and Co = 58.933 gms ).

Let A be the weight of  $\text{Sm}_2\text{Co}_{17}$  before nitrogenation,

B be the weight of  $\text{Sm}_2\text{Co}_{17}$  after nitrogenation

and x be the number of nitrogen per mole in the  $\text{Sm}_2\text{Co}_{17}$  after nitrogenation.

Then, the number of mole of nitrogen of  $\text{Sm}_2\text{Co}_{17}$  before nitrogenation is  $\frac{A}{1302.66}$ .

After nitrogenation, the weight of  $\text{Sm}_2\text{Co}_{17}\text{N}_x$  is

$$B = \frac{A}{1302.66} [1302.66 + 14.007x] \quad (\text{N} = 14.007 \text{ gms}) \quad (\text{A.1})$$

From equation (A.1), we can find the value of x as

$$x = \frac{1302.66}{14.007} \left( \frac{B}{A} - 1 \right) \quad (\text{A.2})$$

## APPENDIX B

### CALCULATION OF LATTICE PARAMETERS

In this thesis, we assumed that  $\text{Sm}_2\text{Co}_{17}$  had the rhombohedral structure. The relation between interplanar spacing  $d$ , diffracted angle  $2\theta$ , the Miller indices  $(hkl)$  and the relative intensities  $I/I_0$  are shown in TABLE B.1. TABLE B.2 gives the equations for interplanar spacing  $d$  of 5 difference types of structures.

By comparing these variables with the ones obtained from the X-ray diffraction pattern, we can calculate lattice parameters (  $a, c$  ) by using least square method. We start by using equation for rhombohedral structure, as

$$\frac{1}{d_i^2} = \frac{4(h_i^2 + h_i k_i + k_i^2)}{3a^2} + \frac{l_i^2}{c^2} \quad (\text{B.1})$$

Let  $1/a = A$  and  $1/c = C$ , take  $1/d_i$  to the other side, sum over all the data, square them and let it be equal to  $\Delta$ ,

$$[\sum_i \frac{4}{3}(h_i^2 + h_i k_i + k_i^2)A^2 + l_i^2 C^2 - d_i^{-2}]^2 = \Delta \quad (\text{B.2})$$

To obtain least squares, the derivative of  $\Delta$  with respect to  $A^2$  and  $C^2$  are set to zero.

Then we get

$$\frac{4}{3}A^2 \sum_i (h_i^2 + h_i k_i + k_i^2)^2 + C^2 \sum_i (h_i^2 + h_i k_i + k_i^2)l_i^2 = \sum_i (h_i^2 + h_i k_i + k_i^2)d_i^{-2} \quad (\text{B.3})$$

$$\frac{4}{3}A^2 \sum_i (h_i^2 + h_i k_i + k_i^2)l_i^2 + C^2 \sum_i l_i^4 = \sum_i l_i^2 d_i^{-2} \quad (\text{B.4})$$

We can write these equations as the matrix,

$$AX = D \quad (B.5)$$

Using Cramer's rules, we will get the answers for lattice parameters ( a,c ). The program of calculating is shown below.



สถาบันวิทยบริการ  
จุฬาลงกรณ์มหาวิทยาลัย

TABLE B.1

XRD data of  $\text{Sm}_2\text{Co}_{17}$  in the Rhombohedral structure

d-value [°A]	( hkl )	angle ( $2\theta$ )	I/I <sub>0</sub>
6.240	101	14.182	5
4.670	012	18.988	5
3.480	021	25.577	5
3.110	202	28.681	5
2.916	113	30.634	50
2.803	104	31.902	20
2.681	211	33.395	5
2.503	122	35.847	10
2.425	300	37.042	60
2.317	024,015	38.836	50
2.098	220	43.081	100
2.081	303	43.451	100
2.041	214	44.347	40
2.025	006,205	44.716	20
1.916	312	47.411	5
1.866	223	48.763	60
1.825	125	49.932	50
1.796	401	50.795	5
1.742	042	52.488	10
1.691	107	54.198	10
1.680	134	54.582	20
1.611	232	57.129	10
1.565	027,404	58.971	10
1.555	306,315	59.388	40
1.477	143	62.870	40
1.466	217,324	63.396	40
1.457	226,045	63.834	60
1.401	330	66.710	40

TABLE B.2  
Equations for d spacings

Monoclinic	$d = \left( \frac{\frac{h^2}{a^2} + \frac{l^2}{c^2} - \frac{2hl \cos \beta}{ac}}{\sin^2 \beta} + \frac{k^2}{b^2} \right)^{-\frac{1}{2}}$
Orthorhombic	$d = \left( \frac{h^2}{a^2} + \frac{k^2}{b^2} + \frac{l^2}{c^2} \right)^{-\frac{1}{2}}$
Hexagonal and rhombohedral	$d = \left( \frac{4}{3} \frac{h^2 + hk + k^2}{a^2} + \frac{l^2}{c^2} \right)^{-\frac{1}{2}}$
Tetragonal	$d = \left( \frac{h^2 + k^2}{a^2} + \frac{l^2}{c^2} \right)^{-\frac{1}{2}}$
Cubic	$d = \frac{a}{(h^2 + k^2 + l^2)^{\frac{1}{2}}}$

สถาบันวิทยบริการ  
จุฬาลงกรณ์มหาวิทยาลัย

## Program Finding the lattice parameters

```

PROGRAM LINEAR_EQUATION;
Const Max=6;
      DataNo=6;
      n=3;
Type
  Matrix = array[1..Max,1..Max] of Real;
  Vector = array[1..Max] of real;
Var
  a,b : Matrix;
  x : Vector;

Function ReadReal(ch:Char;n:Byte):Real;
var x:Real;
begin
  Write('Input ',ch,[' ',n,'] : '); ReadLn(x);
  ReadReal:=x;
end;

Procedure Input;
var i,j,k : integer;
begin
  writeln('Input data');
  for i := 1 to DataNo do
  begin
    b[i,1]:=ReadReal('n',i);
    b[i,2]:=ReadReal('m',i);
    b[i,3]:=ReadReal('l',i);
    b[i,4]:=ReadReal('e',i);
  end;
  for i:=1 to 4 do
  for j:=1 to 4 do
    a[i,j]:=0;
    for k:=1 to DataNo do
      begin
{ Matrix A }
        a[1,1]:=a[1,1]+4/3*Sqr(Sqr(b[k,1])+b[k,1]*
b[k,2]+Sqr(b[k,2]));
        a[1,2]:=a[1,2]+(Sqr(b[k,1])+b[k,1]*b[k,2]+
Sqr(b[k,2]))*Sqr(b[k,3]);
        a[2,1]:=a[2,1]+4/3*(Sqr(b[k,1])+b[k,1]*b
[k,2]+Sqr(b[k,2]))*Sqr(b[k,3]);
        a[2,2]:=a[2,2]+Sqr(Sqr(b[k,3]));
          end;
        for i:=1 to 2 do
          x[i]:=0;
          for k:=1 to DataNo do
            begin

```

```

{ Matrix D }
          x[1]:=x[1]+(Sqr(b[k,1])+b[k,1]*b
[k,2]+Sqr(b[k,2]))*Sqr(2*
          Sin(Pi*b[k,4]/360)/1.5406);
          x[2]:=x[2]+Sqr(b[k,3])*2*Sqr(Sin(Pi*b
[k,4]/360)/1.5406);
          end;

{ Using Cramer's rule }

a[4,4]:=a[1,1]*a[2,2]-a[2,1]*a[1,2], { det A }
a[3,4]:=x[1]*a[2,2]-x[2]*a[1,2]/a[4,4];
a[4,3]:=a[1,1]*x[2]-a[2,1]*x[1]/a[4,4];
writeln;
writeln('Lattice parameter a = ',
1/sqrt(a[3,4]));
writeln('Lattice parameter c = ',
1/sqrt(a[4,3]));

end; {Input}

BEGIN {main}
  Input;
END.

```

## CURRICULUM VITAE



Miss Narumon Suwonjandee was born on August 24, 1970 in Bangkok. She was earned a B.Sc.degree in Physics from Chulalongkorn University in 1992.



สถาบันวิทยบริการ  
จุฬาลงกรณ์มหาวิทยาลัย